Interfaces with Other Disciplines

Multivariate FX models with jumps: Triangles, Quantos and implied correlation

Laura Ballotta [a,*], Griselda Deelstra [b], Grégory Rayée [c]

[a] *Cass Business School, City, University of London, United Kingdom*
[b] *Department of Mathematics, ECARES, Université libre de Bruxelles, Belgium*
[c] *Department of Mathematics, SBS-EM, ECARES, Université libre de Bruxelles, Belgium*

ABSTRACT

We propose an integrated model of the joint dynamics of FX rates and asset prices for the pricing of FX derivatives, including Quanto products; the model is based on a multivariate construction for Lévy processes which proves to be analytically tractable. The approach allows for simultaneous calibration to market volatility surfaces of currency triangles, and also gives access to market consistent information on dependence between the relevant variables. A successful joint calibration to real market data is presented for the particular case of the Variance Gamma process.

© 2017 Elsevier B.V. All rights reserved.

1. Introduction

The aim of this paper is to introduce an extended multivariate model for FX rates and equity indices based on Lévy processes, with the aim of recovering market consistent information on the correlation between financial assets using suitable derivatives contracts.

The interest in market implied metrics of correlation is motivated by the fact that correlation risk is attracting interest for hedging and regulatory purposes. This risk is in fact present in the trading books of a wide range of buy and sell side market participants, such as bank structuring desks and hedge funds for example. Further, the Basel III supervisory regime (Basel, 2010) is focusing in particular on the impact of wrong-way risk effects on the quantification of counterparty credit risk through metrics such as Credit Value Adjustment (CVA), wrong-way risk denoting the dependence between the counterparty credit worthiness and the value of the investor's position. Capturing correlation risk requires both suitable models for the joint distribution of the relevant variables, and easy-to-implement procedures for the quantification of the parameters controlling the behavior of the joint distribution of choice. Specifically, regarding the latter issue, we note that possible information sources are either past observed values of the variables in question, or derivatives whose quoted

price offers an estimate of the market perception of correlation. The estimation of historical correlation from time series though is significantly affected by the length of the sample, the frequency of observation and the weights assigned to past observations. Further, as historical measures are backward-looking, they do not necessarily reflect market expectations of future joint movements in the financial quantities of interest, which are instead necessary for the assessment of derivatives positions and related capital requirements. Alternatively, over the past few years the CBOE has made available daily quotes of the CBOE S&P 500 Implied Correlation Index (Chicago Board Options Exchange, 2009), which replaces all pairwise correlations with an average one. Although this index in general reflects market capitalization, it might not be suitable for example for pricing and assessing counterparty credit risk, due to the equi-correlation assumption.

In light of the previous considerations, our analysis is based on traded multivariate derivative products linked to the existing level of correlation. In particular, we focus on the case of the FX market; due to the presence of currency triangles, liquid options on FX rates, including cross rates, and more sophisticated structures such as Quanto products, the FX market does indeed offer a wide range of derivatives contracts which are exposed to correlation risk and, at the same time, supported by sufficient liquidity. Quanto products are, in fact, financial products with a payoff paid in a different currency from the one in which the underlying asset is traded, allowing investors to participate in the assets profit without facing any exposure to foreign exchange rate risk. Due to these features, such contracts are particularly popular in those markets

* Corresponding author.
 E-mail address: L.Ballotta@city.ac.uk (L. Ballotta).

in which the provision of investments in foreign assets is tightly governed by exchange control regulations; this is for example the case in South Africa where commodity investments, such as crude oil, must be listed and settled in South African Rand, although the commodity itself is a dollar-denominated asset.

The choice of using Lévy processes as building blocks for the multivariate FX model is justified by the following considerations. In first place, as reported in the literature, implied correlation – similarly to implied volatility – shows skew patterns (see Da Fonseca, Grasselli, and Tebaldi, 2007; Ballotta and Bonfiglioli, 2016, and references therein, for example) which are not fully consistent with the standard framework based on the Brownian motion, i.e. the Gaussian distribution. Lévy processes represent a simple but effective way of replacing the Gaussian distribution, as many analytical formulas established for models based on the Brownian motion can be easily extended to this more general class of processes. Secondly, we note that the features of asymmetry and excess kurtosis typical of the distributions generated by Lévy processes are consistent with empirical evidence provided for example by Carr and Wu (2007). Thirdly, for a consistent pricing of FX derivatives the multivariate model of choice needs to show symmetries with respect to inversion and triangulation (see De Col, Gnoatto, and Grasselli, 2013, for example); as Lévy processes are invariant under linear transformation, the required symmetries are therefore automatically preserved. Application of Lévy processes for FX modeling at univariate level is relatively well established in the literature, see for example Eberlein and Koval (2006) and references therein.

Multivariate constructions for Lévy processes have attracted interest in the literature over the past few years, for example for modeling and pricing counterparty credit risk (see Lipton and Sepp, 2009; Ballotta and Fusai, 2015, for example). Although several approaches are available, for a detailed survey of which we refer for example to Itkin and Lipton (2015), Luciano, Marena, and Semeraro (2016) and references therein, in the following we adopt the factor construction of Ballotta and Bonfiglioli (2016), in which the overall risk is split in two components: a systematic one originated by sudden changes affecting the whole market (which is also consistent with the results of Atanasov & Nitschka, 2015), and an idiosyncratic one capturing instead shocks originated by asset specific issues. This factor construction also implies that the model shows a flexible correlation structure, a linear dimensional parameter complexity, and readily available characteristic functions, which guarantee a high ease of implementation, and facilitate an integrated calibration procedure providing access to information on the dependence structure between the relevant components. We point out that although our framework is based on the model of Ballotta and Bonfiglioli (2016), in which convolution conditions required to recover a known distribution for the margin processes are derived and applied, our model does not need these restrictive conditions, as they are not necessary to retain its mathematical tractability and a limited number of parameters. As observed for example by Eberlein, Frey, and von Hammerstein (2008), in fact, the presence of convolution conditions aimed at separating the behavior of the margin processes from the correlation structure, although intuitive, leads to a biased view of the dependence in place and reduces the flexibility of the factor model as it fails to recognize the different tail behavior shown by the components of any given multivariate vector. This particular feature distinguishes this approach from the constructions based on multivariate subordinators as for example in Luciano et al. (2016).

In light of the discussion above, this paper offers the following contributions. Firstly, we develop a Lévy processes-based multivariate extended FX framework, which includes additional names to cater for the underlying assets of Quanto products such as Quanto futures and Quanto options. The proposed framework is very general as it can be applied to any class of Lévy processes admitting closed form expressions for their characteristic function. Secondly, we show that the part of the framework concerning the multivariate FX model satisfies symmetries with respect to inversion and triangulation. We note that although these properties are important in order to guarantee a fully consistent FX model, it is not trivial to preserve them once we move out of the standard Black–Scholes framework to allow for more realistic stylized features; for further details on this matter, we refer for example to De Col et al. (2013). Concerning non-Gaussian frameworks for Quanto products, we cite amongst others Branger and Muck (2012), who offer an integrated pricing approach for both Quanto and plain-vanilla options on the stock as well as the foreign exchange rate based on Wishart processes. Thirdly, the proposed model leads to analytical results (up to a Fourier inversion) for the price of both vanilla and Quanto options, which allow for efficient calibration to market quotes in almost real time for both FX triangles and Quanto products. Finally, our model gives access to analytical formulae for the correlation coefficient and the indices of tail dependence, which facilitate the recovery of market implied correlation and the assessment of joint movements on the risk position of investors.

In Section 2, we review the general features of the factor-based multivariate Lévy processes, with particular attention to the results required for the construction of the multivariate FX model, which is introduced in Section 3. In Section 3, we also introduce calibration procedures based on FX triangles and Quanto futures. The numerical analysis is offered in Section 4 together with some considerations on implications on risk management and capital requirements. Section 5 concludes. All the proofs are deferred to the on-line companion.

2. Preliminaries: multivariate Lévy processes via linear transformation

The aim of this section is to provide a comprehensive review of the main results regarding multivariate Lévy processes obtained by linear transformation, which will be used for the construction of the multivariate FX model of Section 3.1, and the pricing results offered in Sections 3.2 and 3.3.

Consider a filtered probability space $\left(\Omega, \mathcal{F}, \{\mathcal{F}_t\}_{t\geq 0}, \mathbb{P}\right)$. Let $\mathbf{L}(t)$ be a Lévy process in $\mathbb{R}^n$, then in virtue of the celebrated Lévy–Khintchine representation its characteristic function is $\phi_{\mathbf{L}}(\mathbf{u}; t) = e^{t\varphi(\mathbf{u})}$ with

$$\varphi(\mathbf{u}) = i\langle \gamma, \mathbf{u}\rangle - \frac{1}{2}\langle \mathbf{u}, \Sigma\mathbf{u}\rangle + \int_{\mathbb{R}^d} (e^{i\langle \mathbf{u}, \mathbf{x}\rangle} - 1 - i\langle \mathbf{u}, \mathbf{x}\rangle 1_E(\mathbf{x}))\kappa(d\mathbf{x}), \tag{1}$$

where $\gamma \in \mathbb{R}^n$, Σ is a symmetric, non-negative definite $n \times n$ matrix capturing the variance/covariance matrix of the Gaussian component, $E = \{\mathbf{x} : |\mathbf{x}| \leq 1\}$, and κ is a positive measure on $\mathbb{R}^n$ such that

$$\kappa(\{0\}) = 0, \quad \int_{\mathbb{R}^d} \left(|\mathbf{x}|^2 \wedge 1\right)\kappa(d\mathbf{x}) < \infty.$$

The triplet (γ, Σ, κ) represents the generating triplet of $\mathbf{L}(t)$ and $\varphi(\cdot)$ denotes the characteristic exponent. For the purpose of the financial model put forward in the following sections, we require in particular the finiteness of the moments of the processes of interest; this is guaranteed if each component of $\mathbf{L}(t)$ satisfies

$$\int_{|x|>1} |x|^p \kappa(dx) < \infty \quad p \in \mathbb{R}^+ \tag{2}$$

(finite absolute pth moment), and

$$\int_{|x|>1} e^{px} \kappa(dx) < \infty \quad p \in \mathbb{R} \tag{3}$$

(finite exponential moment), see Sato (1999, Theorem 25.3) for example. In particular, the finiteness of exponential moments of order 1 can be achieved if the process satisfies

$$\int_{|x|>1} e^{ux} \kappa(dx) < \infty \quad \text{for all } u \in [-M, M], M > 1 \tag{4}$$

where M is a constant, see for example Eberlein (2013) and references therein. In this framework, the elements of the variance/covariance matrix of the process $\mathbf{L}(t)$ are of the form

$$\mathbb{C}ov(L_j(t), L_k(t)) = \left(\Sigma_{jk} + \int_{\mathbb{R}^d} x_j x_k \kappa(dx_j \times dx_k) \right) t \ \ j, k = 1, \dots, n.$$

Further, the indices of skewness and excess kurtosis of each component of $\mathbf{L}(t)$ are respectively

$$skew(t) = \frac{\int_{\mathbb{R}} x^3 \kappa(dx)}{\left(\Sigma_{jj} + \int_{\mathbb{R}} x^2 \kappa(dx) \right)^{3/2} \sqrt{t}},$$

$$kurt(t) = \frac{\int_{\mathbb{R}} x^4 \kappa(dx)}{\left(\Sigma_{jj} + \int_{\mathbb{R}} x^2 \kappa(dx) \right)^2 t}.$$

Hence, the distribution of a Lévy process is always leptokurtic and it can be asymmetric; these features are specifically controlled by the jump size distribution.

In order to construct a multivariate Lévy process with dependent components and explicit representation of the characteristic triplet, we use the property that these processes are invariant under linear transformations (see for example Sato, 1999, Proposition 11.10, and Cont and Tankov, 2004, Theorem 4.1). Specifically, with the aim of providing a full argument for the core of the paper, in the following we revisit and elaborate the results presented in Ballotta and Bonfiglioli (2016).

Proposition 1. Let $\Lambda(t) = (Y_1(t), \dots, Y_n(t), Z(t))^\top$ be a Lévy process in $\mathbb{R}^{n+1}$ with mutually independent components, each with characteristic functions $\phi_{Y_j}(u; t)$, $j = 1, \dots, n$, and $\phi_Z(u; t)$ respectively, and generating triplets $(\beta_j, \sigma_j, \nu_j)$, $j = 1, \dots, n$, and $(\beta_Z, \sigma_Z, \nu_Z)$. Then, for $a_j \in \mathbb{R}$, $j = 1, \dots, n$, $\mathbf{L}(t) = (Y_1(t) + a_1 Z(t), \dots, Y_n(t) + a_n Z(t))^\top$ is a multivariate Lévy process in $\mathbb{R}^n$ with characteristic function

$$\phi_{\mathbf{L}}(\mathbf{u}; t) = \phi_Z \left(\sum_{j=1}^n a_j u_j; t \right) \prod_{j=1}^n \phi_{Y_j}(u_j; t),$$

and generating triplet (γ, Σ, κ) such that

- $\gamma \in \mathbb{R}^n$, $\gamma = (\beta_1 + a_1 \beta_Z, \dots, \beta_n + a_n \beta_Z)^\top + \int_{\mathbb{R}^n} \mathbf{x}(1_E(\mathbf{x}) - 1_D(\mathbf{x})) \kappa(d\mathbf{x})$, for $E = \{\mathbf{x} \in \mathbb{R}^n : \sum_{j=1}^n x_j^2 \leq 1\}$ and $D = \{(y_1 + a_1 z, \dots, y_n + a_n z) \in \mathbb{R}^n : \sum_{j=1}^n y_j^2 + z^2 \leq 1\}$,
- Σ is a $n \times n$ matrix with entries $\Sigma_{jj} = \sigma_j^2 + a_j^2 \sigma_Z^2$ and $\Sigma_{jk} = a_j a_k \sigma_Z^2$ for all $j \neq k$,
- $\kappa(B) = \sum_{j=1}^n \nu_j(B_j) + \nu_Z(B_a)$,

for $B \in \mathcal{B}(\mathbb{R}^n)$,

$$B_j = \{y \in \mathbb{R} : (\underbrace{0, \dots, 0}_{j-1 \text{ times}}, y, \underbrace{0, \dots, 0}_{n-j \text{ times}}) \in B\},$$

$B_a = \{z : z \in A\}$ and $A = \{z \in \mathbb{R} : (a_1 z, \dots, a_n z) \in B\}$.

Proof. See Appendix A.1. □

Corollary 2. Let $\mathbf{L}(t)$ be a $\mathbb{R}^n$ - Lévy process as constructed in Proposition 1, with generating triplet (γ, Σ, κ). Then, for $j = 1, \dots, n$, $L_j(t)$ is a Lévy process in $\mathbb{R}$ with triplet $(\gamma_{Lj}, c_j^2, \kappa_j)$ defined as

- $\gamma_{Lj} = \gamma_j + \int_{\mathbb{R}^n} x_j (1_{x_j^2 \leq 1} - 1_{\sum_{j=1}^n x_j^2 \leq 1}) \kappa(d\mathbf{x})$
- $c_j^2 = \sigma_j^2 + a_j^2 \sigma_Z^2$
- $\kappa_j(B) = \kappa(\{\mathbf{x} : x_j = y_j + a_j z \in B\}) = \nu_j(B_j) + \nu_Z(B_{aj})$ for $B \in \mathcal{B}(\mathbb{R})$, $B_j = \{y_j \in \mathbb{R} : y_j \in B\}$, $B_{aj} = \{z \in \mathbb{R} : z \in A_j\}$ and $A_j = \{z \in \mathbb{R} : a_j z \in B\}$.

Proof. See Appendix A.2. □

For the case of the proposed construction, the dependence between components of the multivariate Lévy process $\mathbf{L}(t)$ is correctly described (see Embrechts, McNeil, and Straumann, 2002, for example) by the pairwise linear correlation coefficient

$$\rho_{jk}^{\mathbf{L}} = \mathbb{C}orr(L_j(t), L_k(t)) = \frac{a_j a_k \mathbb{V}ar(Z(1))}{\sqrt{\mathbb{V}ar(L_j(1))} \sqrt{\mathbb{V}ar(L_k(1))}}, \tag{5}$$

which is well defined as all processes have finite moments of second order due to the condition in Eq. (2). For further details on the dependence structure, we refer to Ballotta and Bonfiglioli (2016).

In terms of tail dependence, the following results apply to the proposed multivariate construction.

Proposition 3. Consider the multivariate process $\mathbf{L}(t)$ generated by Proposition 1. Then

(a) For $l_j, l_k \downarrow -\infty$ $j \neq k$, $j = 1, \dots, n$, $\mathbb{P}(L_j(t) < l_j, L_k(t) < l_k) > 0$ for all $t > 0$ if and only if $\rho_{jk}^{\mathbf{L}} > 0$, and

$$\mathbb{P}(L_j(t) < l_j, L_k(t) < l_k) \simeq \begin{cases} \mathbb{P}\left(Z(t) < \min \left\{ \frac{l_j}{a_j}, \frac{l_k}{a_k} \right\} \right) & \text{if } a_j, a_k > 0 \\ \mathbb{P}\left(Z(t) > \max \left\{ \left| \frac{l_j}{a_j} \right|, \left| \frac{l_k}{a_k} \right| \right\} \right) & \text{if } a_j, a_k < 0. \end{cases} \tag{6}$$

(b) For $l_j, l_k \uparrow \infty$ $j \neq k$, $j = 1, \dots, n$, $\mathbb{P}(L_j(t) > l_j, L_k(t) > l_k) > 0$ for all $t > 0$ if and only if $\rho_{jk}^{\mathbf{L}} > 0$, and

$$\mathbb{P}(L_j(t) > l_j, L_k(t) > l_k) \simeq \begin{cases} \mathbb{P}\left(Z(t) > \max \left\{ \frac{l_j}{a_j}, \frac{l_k}{a_k} \right\} \right) & \text{if } a_j, a_k > 0 \\ \mathbb{P}\left(Z(t) < \min \left\{ -\frac{l_j}{|a_j|}, -\frac{l_k}{|a_k|} \right\} \right) & \text{if } a_j, a_k < 0. \end{cases} \tag{7}$$

Proof. See Appendix A.3. □

The above proposition shows that the tail dependence behavior is governed by the tail probabilities of the systematic risk process. Further, results (a) and (b) imply that the indices of upper/lower tail dependence are different from zero only when the margin processes are positively correlated, which is consistent with the fact that these coefficients provide a measure of concordance of jumps (see Embrechts, McNeil, and Straumann, 2002).

We conclude this section by revisiting the results presented in Eberlein, Papapantoleon, and Shiryaev (2009) for the multivariate construction given in Proposition 1. In particular, we consider the case of an Esscher probability measure (see Gerber & Shiu, 1994, for example) $\mathbb{P}^{hj}$ with parameter $h_j \in \mathbb{R}$ defined with respect to the jth component of the vector $\mathbf{L}(t)$. We note that in virtue of condition (2) the "big" jumps of all the relevant Lévy processes have finite first moment (i.e. $\int_{|x| > 1} x\nu(dx) < \infty$); this implies that we can compensate them to form a martingale. Consequently, the processes have triplets $(\gamma'_{Lj} = \gamma_{Lj} + \int_{|x|>1} x\nu(dx), c_j^2, \kappa_j)$, $(\beta'_j = \beta_j + \int_{|y|>1} y\nu(dy), \sigma_j^2, \nu_j)$ for $j = 1, \dots, n$ and $(\beta'_Z = \beta_Z + \int_{|z|>1} z\nu(dz), \sigma_Z^2, \nu_Z)$. For sake of simplicity, we suppress the notation γ', β' and write $\gamma_\cdot$, $\beta_\cdot$ instead. The characteristic exponents now take form

$$\varphi_{Lj}(u) = iu\gamma_{Lj} - \frac{u^2}{2} c_j^2 + \int_{\mathbb{R}} (e^{iux} - 1 - iux) \kappa_j(dx) \quad j = 1, \dots, n$$

Table 1

Entries summarize the characteristic exponent for each Lévy process specification under both $\mathbb{P}$ and the Esscher measure of parameter h, $\mathbb{P}^h$.

Lévy process	$\mathbb{P}$-characteristic exponent $\varphi(u)$	$\mathbb{P}^h$-characteristic exponent $\varphi^h(u)$
Arithmetic Brownian motion	$iu\mu - \frac{u^2}{2}\sigma^2$	$iu\mu^h - \frac{u^2}{2}\sigma^2$
	$\mu \in \mathbb{R}, \sigma > 0$	$\mu^h = \mu + h\sigma^2$
Variance Gamma (VG)	$-\frac{1}{k}\ln(1 - iu\theta k + \frac{u^2}{2}\sigma^2 k)$	$-\frac{1}{k}\ln(1 - iu\theta^h k^h + \frac{u^2}{2}\sigma^2 k^h)$
Madan et al. (1998)	$\theta \in \mathbb{R}, \sigma, k > 0$	$\theta^h = \theta + h\sigma^2, \; k^h = k(1 - h\theta k - \frac{h^2}{2}\sigma^2 k)^{-1}$
Normal Inverse Gaussian (NIG)	$\frac{1}{k}(1 - \sqrt{1 - 2iu\theta k + u^2\sigma^2 k})$	$\frac{1}{\sqrt{kk^h}}(1 - \sqrt{1 - 2iu\theta^h k^h + u^2\sigma^2 k^h})$
Barndorff-Nielsen (1995)	$\theta \in \mathbb{R}, \sigma, k > 0$	$\theta^h = \theta + h\sigma^2, \; k^h = k(1 - 2h\theta k - h^2\sigma^2 k)^{-1/2}$
Merton Jump Diffusion	$iu\mu - \frac{u^2}{2}\sigma^2 + \lambda(e^{iu\alpha - \frac{u^2}{2}\beta^2} - 1)$	$iu\mu^h - \frac{u^2}{2}\sigma^2 + \lambda^h(e^{iu\alpha^h - \frac{u^2}{2}\beta^2} - 1)$
Merton (1976)	$\mu, \alpha \in \mathbb{R}, \sigma, \beta > 0$	$\mu^h = \mu + h\sigma^2, \; \lambda^h = \lambda e^{h\alpha + \frac{h^2}{2}\beta^2}, \; \alpha^h = \alpha + h\beta^2$
CGMY	$C\Gamma(-Y)\big((G + iu)^Y - G^Y$	$C\Gamma(-Y)\big((G^h + iu)^Y - (G^h)^Y$
Carr, Geman, Madan, and Yor (2002)	$+(M - iu)^Y - M^Y\big)$	$+(M^h - iu)^Y - (M^h)^Y\big)$
	$C > 0, G, M \geq 0, Y < 2$	$M^h = M - h, \; G^h = G + h$

$$\varphi_{Y_j}(u) = iu\beta_j - \frac{u^2}{2}\sigma_j^2 + \int_{\mathbb{R}}\left(e^{iuy} - 1 - iuy\right)\nu_j(dy) \quad j = 1, \ldots, n$$

$$\varphi_Z(u) = iu\beta_Z - \frac{u^2}{2}\sigma_Z^2 + \int_{\mathbb{R}}\left(e^{iuz} - 1 - iuz\right)\nu_Z(dz).$$

The Esscher change of measure is formalized in the following.

Proposition 4. *Let $\mathbf{\Lambda}(t)$ and $\mathbf{L}(t)$ be multivariate Lévy processes as given in Proposition 1; further, let $\mathbb{P}^{h_j}$ be an equivalent probability measure defined by the density process*

$$\eta(t) = \frac{d\mathbb{P}^{h_j}}{d\mathbb{P}}\bigg|_{\mathcal{F}_t} = e^{-\varphi_{L_j}(-ih_j)t + h_j L_j(t)}, \quad h_j \in \mathbb{R},$$

for any $j = 1, \ldots, n$. Then, $\mathbf{\Lambda}(t)$ and $\mathbf{L}(t)$ remain Lévy processes under $\mathbb{P}^{h_j}$.

Further, the components of $\mathbf{\Lambda}(t)$ under $\mathbb{P}^{h_j}$ for any $j = 1, \ldots, n$ have characteristic exponent

$$\varphi_{Y_j}^{h_j}(u) = iu\left(\beta_j + h_j\sigma_j^2 + \int_{\mathbb{R}} y(e^{h_j y} - 1)\nu_j(dy)\right)$$

$$- \frac{u^2}{2}\sigma_j^2 + \int_{\mathbb{R}}\left(e^{iuy} - 1 - iuy\right)e^{h_j y}\nu_j(dy)$$

$$\varphi_{Y_k}^{h_j}(u) = \varphi_{Y_k}(u), \quad k \neq j, k = 1, \ldots, n$$

$$\varphi_Z^{h_j}(u) = iu\left(\beta_Z + h_j a_j\sigma_Z^2 + \int_{\mathbb{R}} z(e^{h_j a_j z} - 1)\nu_Z(dz)\right)$$

$$- \frac{u^2}{2}\sigma_Z^2 + \int_{\mathbb{R}}\left(e^{iuz} - 1 - iuz\right)e^{h_j a_j z}\nu_Z(dz).$$

Proof. See Appendix A.4 □

The corresponding characteristic exponents of the components of $\mathbf{L}(t)$ under $\mathbb{P}^{h_j}$ follow from Proposition 1 and Corollary 2 (see also Eberlein et al., 2009).

Proposition 4 implies that Lévy processes are invariant under an Esscher change of measure; in other words any Lévy process remains Lévy after an appropriate redefinition of the process parameters. As an illustration, we list in Table 1 the characteristic function under both $\mathbb{P}$ and $\mathbb{P}^{h_j}$ of some of the Lévy processes most commonly used for financial applications.

A direct consequence of Proposition 4 (and the condition in Eq. (4)) is

$$\mathbb{E}^{h_j}\left(e^{L_k(t) - t\varphi_{L_k}(-i)}\right) = e^{q_{h_j} t} \quad k \neq j \tag{8}$$

with

$$q_{h_j} = h_j \mathbb{C}ov\big(L_k(1), L_j(1)\big) + \sum_{n=3}^{\infty}\sum_{l=1}^{n-1}\frac{a_k^{n-l}h_j^l a_j^l}{l!(n-l)!}\int_{\mathbb{R}} z^n\nu_Z(dz). \tag{9}$$

The result follows from the Taylor expansion of the exponential function about the origin and the binomial theorem. This result

will be useful in Section 3.3.1 in order to gauge the impact of dependence on the so called 'Quanto adjustment'.

Unless otherwise stated, all the assumptions listed in this section hold throughout the rest of the paper.

3. A multivariate Lévy (extended) foreign exchange market

3.1. The general setting

Consider a frictionless and arbitrage free market in which N currencies are traded. In what follows, we use the convention that the spot FX rate between the lth and the mth currency, $X^{m|l}(t)$, is quoted as the amount of currency (l) per unit of currency (m). Further, we assume that interest rates are constant and we let $r_l > 0$, $l = 1, \ldots, N$ denote the continuously compounded interest rate in the lth currency.

For the purpose of including the pricing of Quanto products, we also consider an asset $S(t)$ traded in the market using the lth currency. Hence, the total number of assets considered is $n = N + 1$. We note that for ease of exposition and notation, in the following we consider only the case of one underlying asset; however, the model can be generalized to the case of say M assets, so that $n = N + M$.

In order to model the risk dynamics of $S(t)$ and $X^{m|l}(t)$, let $(L_S(t), L_{X_{k|l}}(t), k \neq l)$ be a Lévy process in $\mathbb{R}^n$ with dependent components and respecting the construction given in Proposition 1, so that

$$L_j(t) = Y_j(t) + a_j Z(t), \quad j = S, X_{k|l}, k \neq l.$$

As shown in Section 2, the full description of $(L_S(t), L_{X_{k|l}}(t), k \neq l)$ depends on the idiosyncratic risk processes $(Y_S(t), Y_{X_{k|l}}(t), k \neq l)$ and the systematic risk process $Z(t)$; hence for simplicity of notation, we focus only on the properties of these components.

Finally, let $\mathbb{P}^l$ be the risk neutral martingale measure defined by the lth currency. We note that the proposed market model is incomplete and consequently the risk neutral martingale measure is not unique. Hence, we follow standard practice for incomplete markets and fix the risk neutral measure with respect to the chosen currency through the prices of derivative contracts traded in the corresponding market. Under this measure, we assume that all processes have zero drift, so that the corresponding generating triplets are $(0, \sigma_j^2, \nu_j)$, for $j = S, X_{k|l}, k \neq l$ and $(0, \sigma_Z^2, \nu_Z)$ respectively, and the characteristic exponents are therefore

$$\varphi_{Y_j}^l(u) = -\frac{u^2}{2}\sigma_j^2 + \int_{\mathbb{R}}(e^{iuy} - 1 - iuy)\nu_j(dy) \quad j = S, X_{k|l}, k \neq l \tag{10}$$

$$\varphi_Z^l(u) = -\frac{u^2}{2}\sigma_Z^2 + \int_{\mathbb{R}}(e^{iuz} - 1 - iuz)\nu_Z(dz). \tag{11}$$

We note that in the interest of highlighting the generality of our approach, in the following we refer to the characteristic exponent $\varphi.(u)$ in its general formulation as from the Lévy–Khintchine representation (see Section 2). For practical purposes, this exponent admits closed form expression in all the cases of processes usually adopted in the finance literature, as the ones reported for example in Table 1.

In this set-up, the index quoted in the lth currency, $S(t)$, and the FX spot rate $X^{m|l}(t)$ under the risk neutral measure $\mathbb{P}^l$ are assumed to be of the form

$$S(t) = S(0)e^{\mu_S t + L_S(t)}, \quad S(0) > 0$$
$$X^{m|l}(t) = X^{m|l}(0)e^{\mu_{X_{m|l}} t + L_{X_{m|l}}(t)}, \quad X^{m|l}(0) > 0$$

with

$$\mu_S = r_l - \varphi^l_{L_S}(-i) = r_l - \varphi^l_{Y_S}(-i) - \varphi^l_Z(-a_{Y_S}i),$$
$$\mu_{X_{m|l}} = r_l - r_m - \varphi^l_{L_{X_{m|l}}}(-i) = r_l - r_m - \varphi^l_{Y_{X_{m|l}}}(-i) - \varphi^l_Z(-a_{X_{m|l}}i).$$

This choice guarantees that $e^{-r_l t}S(t)$ and $e^{-(r_l - r_m)t}X^{m|l}(t)$ (i.e. the discounted value of one unit of currency (m) invested in the m-denominated currency money market account and converted in the (l) currency) are $\mathbb{P}^l$-martingales.

Up to now, the given market is specified under the risk neutral measure defined by the lth currency; for practical purposes it is at times convenient to change the measure to any other one based on a numéraire denominated in any other of the N currencies included in the FX market. Without loss of generality, we consider the risk neutral martingale measure defined by the mth currency. In the given framework, due to the change-of-numéraire method introduced by Geman, El Karoui, and Rochet (1995), $\mathbb{P}^m \sim \mathbb{P}^l$ is defined by the density process

$$\eta(t) = \left.\frac{d\mathbb{P}^m}{d\mathbb{P}^l}\right|_{\mathcal{F}_t} = \frac{e^{r_m t}X^{m|l}(t)}{e^{r_l t}X^{m|l}(0)}$$
$$= e^{-\varphi^l_{L_{X_{m|l}}}(-i)t + L_{X_{m|l}}(t)}. \tag{12}$$

As $\mathbb{P}^m$ can be considered an Esscher probability measure with unit parameter, it follows from Proposition 4 that the spot FX log-rate and the log-returns of the index $S(t)$ remain Lévy processes under the change of measure; the corresponding characteristic exponents under the probability measure $\mathbb{P}^m$, denoted by $\varphi.^m$, follow directly from Proposition 4.

$$\varphi^m_{Y_{X_{m|l}}}(u) = iu\left(\sigma^2_{X_{m|l}} + \int_{\mathbb{R}} y(e^y - 1)\nu_{X_{m|l}}(dy)\right)$$
$$- \frac{u^2}{2}\sigma^2_{X_{m|l}} + \int_{\mathbb{R}}(e^{iuy} - 1 - iuy)e^y\nu_{X_{m|l}}(dy) \tag{13}$$

$$\varphi^m_{Y_j}(u) = -\frac{u^2}{2}\sigma^2_j + \int_{\mathbb{R}}(e^{iuy} - 1 - iuy)\nu_j(dy) \quad j = S, X_{k|l}, k \neq l, m \tag{14}$$

$$\varphi^m_Z(u) = iu\left(a_{X_{m|l}}\sigma^2_Z + \int_{\mathbb{R}} z(e^{a_{X_{m|l}}z} - 1)\nu_Z(dz)\right) - \frac{u^2}{2}\sigma^2_Z$$
$$+ \int_{\mathbb{R}}(e^{iuz} - 1 - iuz)e^{a_{X_{m|l}}z}\nu_Z(dz). \tag{15}$$

In the case of the processes considered in Table 1, these exponents admit closed form expressions reported in the last column of Table 1 by setting $h = 1$.

We note that the proposed multivariate FX model is consistent in terms of symmetries with respect to inversion and triangulation. The result is formalized in the following.

Proposition 5.

(a) *Symmetry with respect to inversion.* Let $X^{l|m}(t) = 1/X^{m|l}(t)$ be the "flipped" FX rate; consider the probability measure $\mathbb{P}^m$ defined by (12). Then under $\mathbb{P}^m$

$$X^{l|m}(t) = X^{l|m}(0)e^{(r_m - r_l - \varphi^m_{L_{X_{l|m}}}(-i))t + L_{X_{l|m}}(t)}, \tag{16}$$

for $L_{X_{l|m}}(t) = Y_{X_{l|m}}(t) + a_{X_{l|m}}Z(t)$, $Y_{X_{l|m}}$ independent of $Z(t)$ and $a_{X_{l|m}} = -a_{X_{m|l}}$. Further, the component processes have characteristic exponents $\varphi^m_{Y_{X_{l|m}}}(u) = \varphi^m_{Y_{X_{m|l}}}(-u)$ and $\varphi^m_Z(u)$ for $\varphi^m_{Y_{X_{m|l}}}(u), \varphi^m_Z(u)$ as in Eqs. (13)–(15).

(b) *Symmetry with respect to triangulation.* Let $X^{m|g}(t) = X^{m|l}(t)/X^{g|l}(t)$ be inferred cross rate; further define $\mathbb{P}^g \sim \mathbb{P}^l$ by

$$\xi(t) = \left.\frac{d\mathbb{P}^g}{d\mathbb{P}^l}\right|_{\mathcal{F}_t} = e^{-\varphi^l_{L_{X_{g|l}}}(-i)t + L_{X_{g|l}}(t)}.$$

Then under $\mathbb{P}^g$

$$X^{m|g}(t) = X^{m|g}(0)e^{(r_g - r_m - \varphi^g_{L_{X_{m|g}}}(-i))t + L_{X_{m|g}}(t)}, \tag{17}$$

for $L_{X_{m|g}}(t) = Y_{X_{m|g}}(t) + a_{X_{m|g}}Z(t)$, $Y_{X_{m|g}}$ independent of $Z(t)$ and $a_{X_{m|g}} = a_{X_{m|l}} - a_{X_{g|l}}$. Further, the component processes have characteristic exponents

$$\varphi^g_{Y_{X_{m|g}}}(u) = \varphi_{Y_{X_{m|l}}}(u) + \varphi^g_{Y_{X_{g|l}}}(-u) \tag{18}$$

$$\varphi^g_{Y_{X_{g|l}}}(u) = iu\left(\sigma^2_{X_{g|l}} + \int_{\mathbb{R}} y(e^y - 1)\nu_{X_{g|l}}(dy)\right)$$
$$- \frac{u^2}{2}\sigma^2_{X_{g|l}} + \int_{\mathbb{R}}(e^{iuy} - 1 - iuy)e^y\nu_{X_{g|l}}(dy) \tag{19}$$

$$\varphi^g_Z(u) = iu\left(a_{X_{g|l}}\sigma^2_Z + \int_{\mathbb{R}} z(e^{a_{X_{g|l}}z} - 1)\nu_Z(dz)\right)$$
$$- \frac{u^2}{2}\sigma^2_Z + \int_{\mathbb{R}}(e^{iuz} - 1 - iuz)e^{a_{X_{g|l}}z}\nu_Z(dz). \tag{20}$$

Proof. See Appendix A.5. $\square$

Same consideration as above holds for the recovery of the characteristic exponents in closed form. These symmetries ensure that for the cases in which options on the inferred rates are actively traded in the market, the proposed model is able to consistently reprice vanilla options written on the different FX rates. The option pricing problem is discussed in the next section.

3.2. Pricing FX options: implied correlation

The framework introduced in the previous section leads to analytical results (up to a Fourier inversion) for the price of vanilla options on FX rates. More precisely, consider a call option on a generic FX rate $X^{m|l}(t)$ struck at $K^{m|l}$ and maturity T. By risk neutral valuation, the option premium (expressed in the relevant lth currency) is

$$C(K^{m|l}, T) = e^{-r_l T}\mathbb{E}^l[(X^{m|l}(T) - K^{m|l})^+]; \tag{21}$$

for the computation of the above, the Carr and Madan (1999) methodology can be adopted so that

$$C(K^{m|l}, T) = \frac{e^{-\alpha \ln K^{m|l}}}{\pi}\int_0^\infty e^{-iv \ln K^{m|l}}\psi^l_{m|l}(v)dv, \tag{22}$$

$$\psi^l_{m|l}(v) = \frac{e^{-r_l T}\phi^l_{m|l}(v - (\alpha+1)i; T)}{\alpha^2 + \alpha - v^2 + i(2\alpha+1)v}, \tag{23}$$

with

$$\phi^l_{m|l}(u; T) = e^{iu \ln X^{m|l}(0) + \left(iu\mu_{X_{m|l}} + \varphi^l_{Y_{m|l}}(u) + \varphi^l_Z(a_{m|l}u)\right)T}, \tag{24}$$

and α a dampening coefficient. The relevant characteristic exponents are obtained by applying Eqs. (10) and (11).

The option pricing Eqs. (22) and (23) show that the FX option price is necessarily a function of both the idiosyncratic and the systematic factors composing the margin process driving the relevant FX rate. This implies that model calibration is non-trivial as these factors are not directly observable in the market. However, in the context of the setting introduced in Section 3, due to the highlighted symmetry with respect to triangulation, the proposed model allows a simple and effective way to solve this problem as, in presence of actively traded options on the inferred cross rates, the required information on the risk factors can be recovered by simultaneous calibration to the three market volatility surfaces. For the case of the cross rate $X^{m|g}(t)$ given in the previous section, in fact, the option pricing formulas (22) and (23) can be restated as

$$C(K^{m|g}, T) = \frac{e^{-\alpha \ln K^{m|g}}}{\pi} \int_0^\infty e^{-iv \ln K^{m|g}} \psi^g_{m|g}(v) dv, \qquad (25)$$

$$\psi^g_{m|g}(v) = \frac{e^{-r_g T} \phi^g_{m|g}(v - (\alpha + 1)i; T)}{\alpha^2 + \alpha - v^2 + i(2\alpha + 1)v}, \qquad (26)$$

where

$$\phi^g_{m|g}(u; T) = e^{iu \ln(X^{m|g}(0)) + \left(iu\mu_{X_{m|g}} + \varphi^g_{Y_{m|g}}(u) + \varphi^g_Z(a_{m|g}u)\right)T}, \qquad (27)$$

$\mu_{X_{m|g}} = r_g - r_m - \varphi^g_{L_{X_{m|g}}}(-i)$, and the relevant characteristic exponents are given by Eqs. (18)–(20).

In more details, consider a generic $m/l/g$ currency triangle; calibration is performed by a non-linear least-squares optimizer minimizing the total calibration error defined in terms of the difference between calibrated and target implied volatilities, denoted σ_{mod} and σ_{mkt} respectively. σ_{mod} is recovered by inversion of the Black–Scholes formula in correspondence of input prices computed using the pricing formulas above. We choose a norm in implied volatility rather than a norm in price as to avoid the introduction of bias due to the large numerical range of option price – for a detailed discussion we refer to De Col et al. (2013) and references therein. Consequently, the objective function of our calibration problem is

$$F(\hat{\theta}) = \sum_i \sum_j \left(\sigma_{mod}\left(X^{m|l}, K_i^{m|l}, T_j; \hat{\theta}_{m|l}\right) - \sigma_{mkt}\left(X^{m|l}, K_i^{m|l}, T_j\right) \right)^2$$
$$+ \sum_i \sum_j \left(\sigma_{mod}\left(X^{g|l}, K_i^{g|l}, T_j; \hat{\theta}_{g|l}\right) - \sigma_{mkt}\left(X^{g|l}, K_i^{g|l}, T_j\right) \right)^2$$
$$+ \sum_i \sum_j \left(\sigma_{mod}\left(X^{m|g}, K_i^{m|g}, T_j; \hat{\theta}\right) - \sigma_{mkt}\left(X^{m|g}, K_i^{m|g}, T_j\right) \right)^2, \qquad (28)$$

where we sum the total number of possible strikes and maturities available for each contract in the dataset (which we omit in the interest of readability). In Eq. (28) $\hat{\theta}$ is an element of the set of feasible vectors Θ defined as

$$\Theta = \{\hat{\theta} = (\mathcal{Y}_{m|l}, \mathcal{Y}_{g|l}, \mathcal{Z}, a_{m|l}, a_{g|l}) \in \mathbb{R}^{\bar{n}_{m|l} + \bar{n}_{g|l} + \bar{n}_Z + 2} \mid c(\hat{\theta})\},$$

where $\mathcal{Y}_{m|l}$, $\mathcal{Y}_{g|l}$ and $\mathcal{Z}$ are the parameter sets describing the idiosyncratic and systematic risk factors of the relevant FX rates, $\hat{\theta}_{m|l}$ and $\hat{\theta}_{g|l}$ refer resp. to the components $\hat{\theta}_{m|l} = (\mathcal{Y}_{m|l}, \mathcal{Z}, a_{m|l})$ and $\hat{\theta}_{g|l} = (\mathcal{Y}_{g|l}, \mathcal{Z}, a_{g|l})$ of $\hat{\theta} \in \Theta$, $\bar{n}.$ is the number of parameters describing the process of choice for the idiosyncratic and systematic factors (from Table 1 we observe, for example, that in the case of the VG process $\bar{n}. = 3$), and $c(\hat{\theta})$ denotes the vector of all possible constraints on the parameters (like the ones listed in Table 1 for the processes presented therein). Finally, the optimization problem used to estimate the model parameters can be stated as

follows

$$\min_{\hat{\theta} \in \Theta} F(\hat{\theta}). \qquad (29)$$

As a result of this procedure, we can also recover as a by product the implied correlation between the relevant FX rates.

3.3. Quanto products: Quanto adjustment and implied correlation

3.3.1. Quanto futures

In the following, we show how to recover market consistent information on the dependence structure between FX rates and the index S via Quanto products. As Quanto futures are the most frequently traded contracts, we analyse their pricing in the proposed setting as to gain insight into the Quanto adjustment.

To this purpose, given that Quanto futures involve only one underlying asset and one FX rate, in the remaining of this paper we consider a reduced version of the multivariate FX market introduced in Section 3.1, with only two currencies: the domestic currency (d), and the foreign (f) currency. Further, for simplicity of notation, we drop the sub-indices from all processes involved, so that under the Foreign Risk Neutral (FRN) martingale measure $\mathbb{P}^f$, the underlying asset price at $t > 0$ is

$$S(t) = S(0)e^{\mu_S^f t + L_S(t)}, \quad S(0) > 0;$$

in accordance with the notation introduced in Section 3.1, the relevant spot FX rate is $X^{d|f}(t)$ defined as

$$X^{d|f}(t) = X^{d|f}(0)e^{\mu_X^f t + L_X(t)}, \quad X^{d|f}(0) > 0,$$

with

$$\mu_S^f = r_f - \varphi_{Y_S}^f(-i) - \varphi_Z^f(-a_S i),$$
$$\mu_X^f = r_f - r_d - \varphi_{Y_X}^f(-i) - \varphi_Z^f(-a_X i).$$

It follows by standard no-arbitrage arguments that the price in the foreign economy at time $t \geq 0$ of the futures on S with maturity T equals

$$F^f(S; t, T) = e^{r_f(T-t)}S(t); \qquad (30)$$

similarly, under the assumption that the applied FX rate between the two currencies is set to 1 d/f (see Giese, 2012, for example), the Quanto futures price in the domestic economy (i.e. under the Domestic Risk Neutral – DRN – martingale measure $\mathbb{P}^d$) is given by

$$F^d(S; t, T) = \mathbb{E}^d[S(T) \mid \mathcal{F}_t]$$
$$= e^{q(T-t)}F^f(S; t, T), \qquad (31)$$

where q is the Quanto adjustment given by

$$q = \mathbb{C}ov^f(L_S(1), L_X(1)) + \sum_{n=3}^\infty \sum_{l=1}^{n-1} \frac{a_S^{n-l}a_X^l}{l!(n-l)!} \int_\mathbb{R} z^n \nu_Z(dz), \qquad (32)$$

in virtue of Eqs. (8) and (9) with $h_j = 1$. In this respect, we note that, in the case in which the driving processes are all Brownian motions (i.e. continuous processes with no jumps), the Quanto adjustment reduces to the well known "Black–Scholes type" Quanto adjustment

$$q = a_S a_X \sigma_Z^2 = \rho_{SX} \sqrt{\mathbb{V}ar(L_X(1))\mathbb{V}ar(L_S(1))}, \qquad (33)$$

and therefore it only depends on the linear pairwise correlation coefficient between the relevant driving processes. In the more general case, though, Eq. (32) shows that the Quanto adjustment also depends on higher order cumulants of the pure jump part of the systematic risk process calculated under $\mathbb{P}^f$. Therefore, as quotes for Quanto futures contracts are readily available from the market, these can be used to calibrate the parameters of the systematic risk

factor, and hence recover information on the "implied" correlation existing between the log-returns of the index and spot FX rate.

The previous observation leads to a 2-step calibration procedure structured as follows. In first place, we assume that in the market there are Quanto futures prices on M different underlying assets $(S_1, \ldots, S_M)$; further, we assume that the M assets are traded in the foreign market with currency f. The Quanto futures are instead cash settled and traded in the domestic currency d. Thus, the first step consists in the calibration of the parameters of the systematic risk process, Z, and the loading factors $(a_1, \ldots, a_M, a_X)$ using Quanto futures. With a similar notation to the one adopted in Section 3.2, this is achieved by defining the objective function $F(\hat{\theta})$ as

$$F(\hat{\theta}) = \sum_i \sum_j \left(\frac{F^d_{mod}(S_i, t, T_j; \hat{\theta}) - F^d_{mkt}(S_i, t, T_j)}{F^d_{mkt}(S_i, t, T_j)} \right)^2, \tag{34}$$

and solving the optimization problem

$$\min_{\hat{\theta} \in \Theta} F(\hat{\theta}) \tag{35}$$

with

$$\Theta = \{\hat{\theta} = (\mathcal{Z}, a_1, \ldots, a_M, a_X) \in \mathbb{R}^{\bar{n}_Z + M + 1} \mid c(\hat{\theta})\}.$$

Conditioned on the parameters values obtained in the first step, the second step is given by $M + 1$ independent minimization problems, one per each asset S and the FX rate, aimed at recovering the parameters of the idiosyncratic components. In more details, we achieve this by calibration to the implied volatility surfaces of the corresponding margin processes; consequently, the relevant objective functions are

$$F_i(\hat{\theta}_{Y_i}) = \sum_k \sum_l \left(\sigma_{mod}\left(S_i, K_{i,k}, T_{i,l}; \hat{\theta}_{Y_i}\right) - \sigma_{mkt}\left(S_i, K_{i,k}, T_{i,l}\right) \right)^2$$
$$i = 1, \ldots, M \tag{36}$$

$$F_X(\hat{\theta}_{Y_X}) = \sum_k \sum_l \left(\sigma_{mod}\left(X^{d|f}, K_k, T_l; \hat{\theta}_{Y_X}\right) - \sigma_{mkt}\left(X^{d|f}, K_k, T_l\right) \right)^2. \tag{37}$$

Note the different norm in Eq. (34); this is to ensure consistency in scale with Eqs. (36) and (37) as to avoid the introduction of bias also in this case (see previous section). The actual calibration is the solution to the optimization problems

$$\min_{\hat{\theta}_{Y_i} \in \Theta_{Y_i}} F_i(\hat{\theta}_{Y_i}), \quad i = 1, \ldots, M \tag{38}$$

$$\min_{\hat{\theta}_{Y_X} \in \Theta_{Y_X}} F_X(\hat{\theta}_{Y_X}) \tag{39}$$

with

$$\Theta_{Y_i} = \{\hat{\theta}_{Y_i} = \mathcal{Y}_i \in \mathbb{R}^{\bar{n}_i} \mid c(\hat{\theta}_{Y_i})\}, \quad i = 1, \ldots, M$$

$$\Theta_{Y_X} = \{\hat{\theta}_{Y_X} = \mathcal{Y}_X \in \mathbb{R}^{\bar{n}_X} \mid c(\hat{\theta}_{Y_X})\}.$$

We note that in the case in which the number of Quanto futures quotes available is less than the dimension of the vector $\hat{\theta}$, the first step of the calibration procedure described above is ill-posed. In this situation, we recommend a joint calibration formulated as follows

$$\min_{\hat{\theta} \in \Theta, \hat{\theta}_{Y_i} \in \Theta_{Y_i}, i=1,\ldots,M, \hat{\theta}_{Y_X} \in \Theta_{Y_X}} F(\hat{\theta}) + \sum_i F_i(\hat{\theta}_{Y_i}) + F_X(\hat{\theta}_{Y_X}). \tag{40}$$

Alternatively to the calibration procedure described above which is essentially based on the idea of recovering information on the dependence in place using Quanto futures, one could instead resort to common market practice of using historical correlation/covariance between the variables of interest. In this case, the objective function will have to be restated in terms of fitting the non diagonal entries of the sample covariance matrix to their theoretical counterpart predicted by the multivariate model. This is achieved by redefining the objective function of the first step described above, i.e. Eq. (34), as follows

$$F_C(\hat{\theta}) = \|\mathbb{C}ov_{mod}(S, X; \hat{\theta}) - \mathbb{C}ov_{mkt}(S, X)\|_F \tag{41}$$

and solving the optimization problem

$$\min_{\hat{\theta} \in \Theta} F_C(\hat{\theta}), \tag{42}$$

where $\|\cdot\|_F$ denotes the Frobenius norm, $\mathbb{C}ov_{mod}(\cdot) = \mathbf{a}\mathbf{a}'\mathbb{V}ar(Z(1))$ is the model covariance matrix between the index log-returns and the FX log-rate, $\mathbb{C}ov_{mkt}(\cdot)$ is the corresponding observed covariance matrix. Similarly to the case described above, if the number of quotes is less than the dimension of $\hat{\theta}$, we recommend a joint calibration similar to what stated in Eq. (40) in which $F(\hat{\theta})$ is replaced by $F_C(\hat{\theta})$.

In order to distinguish between the two procedures in the following sections, the calibration based on the optimization problems (35), (38), (39) (alternatively (40)) is referred to as 'QF-based calibration'; instead, we refer to the calibration which uses the optimization problem (42) as first step as 'HC-based calibration'.

3.3.2. Pricing Quanto options

In this section we provide a possible way of back-testing the QF-based and HC-based calibration procedures introduced in the previous section. The idea is to verify the consistency of the information retrieved from the two procedures using the prices of other Quanto products such as Quanto options.

The arbitrage free price of a (European type) Quanto call option on the (Quanto) futures on the asset S, expressed in units of domestic currency, is given by

$$QC(F^d(S; T_1, T_2), K, T_1) = e^{-r_d T_1} \mathbb{E}^d[(F^d(S; T_1, T_2) - K)^+]$$

where $F^d(S; T_1, T_2)$ is the Quanto futures price at time T_1 with maturity T_2; $T_1 \leq T_2$ is the maturity of the option contract.

It follows from Eq. (31) that

$$QC(F^d(S; T_1, T_2), K, T_1) = e^{-r_d T_1} Q_{adj} \mathbb{E}^d[(S(T_1) - K^*)^+] \tag{43}$$

with

$$Q_{adj} = e^{(r_f + q)(T_2 - T_1)},$$

$$K^* = \frac{K}{Q_{adj}}.$$

A Quanto call option can therefore be seen as a vanilla call on S struck at K^*, rescaled by a constant, Q_{adj}, incorporating the Quanto adjustment. As in the market model under consideration relevant characteristic functions are available (see for example Table 1), the price in Eq. (43) can be computed efficiently by means of Fourier inversion based methods, such as the Carr–Madan approach (Carr & Madan, 1999) for example. In this respect, we note that the large majority of options offered on the CME are of American type; the early exercise property can be accommodated in the pricing by adopting either the CONV method of Lord, Fang, Bervoets, and Oosterlee (2008) or the COS method of Fang and Oosterlee (2009) for example; alternatively the so called extension method of Fabozzi, Paletta, Stanescu, and Tunaru (2016) could be used as well. This is left though to future research.

4. Numerical results

4.1. Setup

In this section, we analyze the performance of our model in terms of calibration, pricing and impact on risk management, using real market quotes. We consider two currency triangles – EUR/USD/CHF as on 17/03/2016 and MXN/USD/ZAR as

Table 2

Synopsis of market data. Source: Bloomberg, CME free web platform (see http://www.cmegroup.com/). $r_{\cdot}$: benchmark interest rates. ρ^h: historical correlation between log-returns estimated on a sample size of 128 days.

March 17, 2016		USDCHF–EURCHF	
USDCHF	$X^{m|l}(0)$	0.96	CHF/USD
EURCHF	$X^{g|l}(0)$	1.09	CHF/EUR
USDEUR	$X^{m|g}(0)$	0.88	EUR/USD
US risk free rate of interest	r_m	0.5%	
EUR risk free rate of interest	r_g	0%	
SWISS risk free rate of interest	r_l	0%	
Historical correlation	$\rho^h_{X^{m|l}X^{g|l}}$	45%	
December 21, 2016		USDZAR–MXNZAR	
USDZAR	$X^{m|l}(0)$	14.0824	ZAR/USD
MXNZAR	$X^{g|l}(0)$	0.6892	ZAR/MXN
USDMXN	$X^{m|g}(0)$	20.4330	MXN/USD
US risk free rate of interest	r_m	0.75%	
South African risk free rate of interest	r_d	7%	
Mexican risk free rate of interest	r_l	5.75 %	
Historical correlation	$\rho^h_{X^{m|l}X^{g|l}}$	56.72%	
June 13, 2014		Nikkei 225–USDJPY	
Nikkei 225	$S(0)$	15097.84	JPY
USDJPY	$X(0)$	102.03	JPY/USD
Japan risk free rate of interest	r_f	0.10%	
US risk free rate of interest	r_d	0.25%	
Nikkei 225 futures (Sept)	$F^f(S; 0, T)$	15030	JPY
Nikkei 225 Quanto futures (Sept)	$F^d(S; 0, T)$	15065	USD
	T	12/09/2014	
Historical correlation	ρ^h_{SX}	28%	
April 15, 2016		BRENT–ZARUSD	
BRENT	$S(0)$	43.72	USD
ZARUSD	$X(0)$	0.0687	USD/ZAR
US risk free rate of interest	r_f	0.5%	
South African risk free rate of interest	r_d	7%	
BRENT futures (May)	$F_1^f(S; 0, T_1)$	43.73	USD
BRENT futures (Aug)	$F_2^f(S; 0, T_2)$	43.79	USD
BRENT Quanto futures (May)	$F_1^d(S; 0, T_1)$	43.78	ZAR
BRENT Quanto futures (Aug)	$F_2^d(S; 0, T_2)$	44.37	ZAR
	T_1	10/05/2016	
	T_2	11/08/2016	
Historical correlation	ρ^h_{SX}	31.4%	

Note: as the benchmark Swiss interest rate is negative at the observation date, we assume this rate to be zero.

on 21/12/2016, and two Quanto futures products – the USD-denominated Quanto futures on the Nikkei 225 index observed on 13/06/2014, and the ZAR-denominated Brent Crude Oil Quanto futures observed on 15/04/2016. The South African Rand (ZAR) and the Mexican Peso (MXN) can be classified as emerging markets currencies.[1] The USD-denominated Quanto futures on the Nikkei 225 index are traded on the CME with quarterly maturities (i.e. March, June, September and December) on the second Friday of the contract month; the minimum price change (tick) is 5 index points. Finally, they are characterized by a multiplier of 5 USD for Dollar-denominated CME Nikkei 225 Futures; for more details see e.g. Co, Kerpel, and Labuszewski (2013). The Brent Crude Oil Quanto futures is traded on the JSE and is a Brent crude oil futures contract that is cash settled and traded in ZAR, but mimics the performance of the foreign referenced USD price of Brent crude oil as traded on NYMEX, a subsidiary of the CME Group Inc. Contract months are February, May, August and November; expiry date is the 15th business day prior to the first business day of the next calendar month. Relevant data are summarized in Table 2. Note that in the interest of space we report the market quotes of the relevant products in Appendix B.

This analysis uses the model calibration procedure introduced in the previous sections; for illustration purposes, we choose as relevant Lévy process the VG process of Madan, Carr, and Chang (1998). In some more details, the VG process is a normal tempered stable process obtained by subordinating a Brownian motion with drift by an independent (unbiased) Gamma process. From Table 1 the characteristic exponent reads

$$\varphi(u) = -\frac{1}{k} \ln\left(1 - iuk\theta + u^2 \frac{\sigma^2}{2} k\right), \quad u \in \mathbb{R}, \tag{44}$$

from which it follows that the process has mean θt and variance $(\sigma^2 + k\theta^2)t$; the indices of skewness and excess kurtosis are

$$skew\,(t) = \frac{\theta\left(3\sigma^2 k + 2\theta^2 k^2\right)}{\left(\sigma^2 + \theta^2 k\right)^{3/2} \sqrt{t}},$$

$$kurt\,(t) = \frac{3k\left(\sigma^4 + 4\sigma^2\theta^2 k + 2\theta^4 k^2\right)}{\left(\sigma^2 + \theta^2 k\right)^2 t}.$$

From the above we observe that the parameter $\theta \in \mathbb{R}$ determines the sign of the skewness of the distribution of the VG process, $\sigma > 0$ controls the overall variance level and $k > 0$ governs the kurtosis or tail heaviness of the distribution.

For the implementation of the market model introduced in Section 3, we assume that both the systematic risk process and all the idiosyncratic risk processes of interest follow a VG

---

[1] See, for example, https://finance.yahoo.com/currency-investing/emerging-markets.

Table 3
Top panel – calibrated parameters of the multivariate VG model. TRIANGLE-based calibration: solution to optimization problems (28) and (29). HC-based calibration: Z, a_S, a_X calibrated using historical correlation (128 days). Bottom panel – moments of the resulting margin distribution. RMSE: percentage of the ATM Delta neutral implied volatility (RMSE actual value in parenthesis) – USDEUR: 0.34% (TRIANGLE-based calibration), 0.46% (HC-based calibration). $\rho^{i,VG}_{X^{m|l}X^{g|l}}$: pairwise correlation coefficient from Eq. (5) and the TRIANGLE-based calibrated parameters. $\rho^{h,VG}_{X^{m|l}X^{g|l}}$: recovered pairwise historical correlation. s, κ: indices of skewness and excess kurtosis as in Cont and Tankov (2004). Data: see Tables 2 and B.1.

	TRIANGLE-based calibration				HC-based calibration			
	Idiosyncratic process		Systematic process		Idiosyncratic process		Systematic process	
	USDCHF	EURCHF			USDCHF	EURCHF		
θ_Y	0.1180	0.0632	θ_Z	−0.2846	θ_Y	0.0172	0.0096	θ_Z	0.0863
σ_Y	0.0724	0.0451	σ_Z	0.3859	σ_Y	0.0665	0.0519	σ_Z	0.2920
κ_Y	0.0326	0.1244	κ_Z	0.1504	κ_Y	0.0690	0.2990	κ_Z	0.0610
a	0.1289	0.1169			a	0.2132	0.1551		
RMSE	0.34%	0.49%	(0.0003)		RMSE	0.46%	0.65%	(0.0004)	
$\rho^{i,VG}_{X^{m|l}X^{g|l}}$		0.3857			$\rho^{h,VG}_{X^{m|l}X^{g|l}}$		0.4486		
	Margin process		Systematic process		Margin process		Systematic process	
	USDCHF	EURCHF			USDCHF	EURCHF		
$\mathbb{E}L(1)$	0.0813	0.0300	$\mathbb{E}Z(1)$	−0.2846	$\mathbb{E}L(1)$	0.0357	0.0230	$\mathbb{E}Z(1)$	0.0863
$\sqrt{\mathbb{V}arL(1)}$	0.0915	0.0688	$\sqrt{\mathbb{V}arZ(1)}$	0.4013	$\sqrt{\mathbb{V}arL(1)}$	0.0913	0.0692	$\sqrt{\mathbb{V}arZ(1)}$	0.2927
$s(L(1))$	0.0270	0.0726	$s(Z(1))$	−0.3120	$s(L(1))$	0.0380	0.0861	$s(Z(1))$	0.0539
$\kappa(L(1))$	0.1051	0.2564	$\kappa(Z(1))$	0.5170	$\kappa(L(1))$	0.0997	0.3309	$\kappa(Z(1))$	0.1850

Table 4
Top panel – calibrated parameters of the multivariate VG model. TRIANGLE-based calibration: solution to optimization problems (28) and (29). HC-based calibration: Z, a_S, a_X calibrated using historical correlation (128 days). Bottom panel – moments of the resulting margin distribution. RMSE: percentage of the ATM Delta neutral implied volatility (RMSE actual value in parenthesis) – USDMXN: 0.17% (TRIANGLE-based calibration), 0.19% (HC-based calibration). $\rho^{i,VG}_{X^{m|l}X^{g|l}}$: pairwise correlation coefficient from Eq. (5) and the TRIANGLE-based calibrated parameters. $\rho^{h,VG}_{X^{m|l}X^{g|l}}$: recovered pairwise historical correlation. s, κ: indices of skewness and excess kurtosis as in Cont and Tankov (2004). Data: see Tables 2 and B.2.

	TRIANGLE-based calibration				HC-based calibration			
	Idiosyncratic process		Systematic process		Idiosyncratic process		Systematic process	
	USDZAR	MXNZAR			USDZAR	MXNZAR		
θ_Y	0.0595	−0.1354	θ_Z	−1.3103	θ_Y	−0.0703	0.0399	θ_Z	1.0205
σ_Y	0.0883	0.0950	σ_Z	1.0729	σ_Y	0.0218	0.1405	σ_Z	0.7126
κ_Y	0.1091	0.0441	κ_Z	0.0582	κ_Y	0.1208	0.0676	κ_Z	0.0423
a	−0.1523	−0.1257			a	0.2558	0.1334		
RMSE	0.12%	0.14%	(0.0002)		RMSE	0.13%	0.15%	(0.0002)	
$\rho^{i,VG}_{X^{m|l}X^{g|l}}$		0.7217			$\rho^{h,VG}_{X^{m|l}X^{g|l}}$		0.5672		
	Margin process		Systematic process		Margin process		Systematic process	
	USDZAR	MXNZAR			USDZAR	MXNZAR		
$\mathbb{E}L(1)$	0.2591	0.0294	$\mathbb{E}Z(1)$	−1.3103	$\mathbb{E}L(1)$	0.1907	0.1761	$\mathbb{E}Z(1)$	1.0205
$\sqrt{\mathbb{V}arL(1)}$	0.1929	0.1721	$\sqrt{\mathbb{V}arZ(1)}$	1.1184	$\sqrt{\mathbb{V}arL(1)}$	0.1928	0.1722	$\sqrt{\mathbb{V}arZ(1)}$	0.7428
$s(L(1))$	0.1589	0.0750	$s(Z(1))$	−0.1990	$s(L(1))$	0.1592	0.0637	$s(Z(1))$	0.1695
$\kappa(L(1))$	0.1397	0.1067	$\kappa(Z(1))$	0.2012	$\kappa(L(1))$	0.1384	0.1077	$\kappa(Z(1))$	0.1462

process respectively with parameters $(\theta_Z, \sigma_Z, k_Z)$ and $(\theta_{Y_j}, \sigma_{Y_j}, k_{Y_j})$ for $j = S, X_{k|l}, k \neq l$, under the relevant probability measure. In particular, we notice that under these assumptions, Eqs. (31) and (32) imply

$$F^d(S; t, T) = F^f(S; t, T)e^{q(T-t)}, \qquad (45)$$

with

$$q = \frac{1}{k_Z}\ln\left(\frac{\left(1 - a_X k_Z \theta_Z - \frac{1}{2}k_Z a_X^2 \sigma_Z^2\right)\left(1 - a_S k_Z \theta_Z - \frac{1}{2}k_Z a_S^2 \sigma_Z^2\right)}{1 - (a_S + a_X)k_Z \theta_Z - \frac{1}{2}k_Z(a_S + a_X)^2 \sigma_Z^2}\right). \qquad (46)$$

The results of the several calibration procedures carried out in this numerical experiment are reported in Tables 3–6. At this stage we pay particular attention to the calibration errors: in order to carry out a meaningful comparison given the different nature of the assets involved (FX rates, market indices and futures), we express the Root Mean Square Error (RMSE) reported in Tables 3–6 as percentage of the ATM (Delta neutral) implied volatility (reported in Appendix B). The calibrations based on market information and the ones based instead on historical information generate relatively similar error for all cases considered in this experiment: the errors, in fact, range from 0.12% (in the case of the USDZAR FX rate) to 1.66% (for the case of the USDJPY FX rate). Although these errors are relatively small, even in the case of emerging markets currencies such as ZAR and MXN generally characterized by significantly higher volatilities, the different source of information used (market vs. historical) has a more subtle impact which is analysed in fuller details in the following sections.

4.2. FX Triangles

We implement the calibration procedure introduced in Section 3.2 for the specific case of the currency triangles EUR/USD/CHF and MXN/USD/ZAR. For this purpose we consider vanilla options on these FX rates with maturity 1 month. Following FX conventions, all quotes, which are taken from Bloomberg, are expressed in terms of Delta; specifically we use the Delta Neutral and the 10 and 25 Delta Call and Put market quotes, which are

Table 5

Top panel – calibrated parameters of the multivariate VG model. QF-based calibration: Z, a_S, a_X calibrated using Quanto futures quotes. HC-based calibration: Z, a_S, a_X calibrated using historical correlation (128 days). Bottom panel – moments of the resulting margin distribution. RMSE: percentage of the ATM (Delta neutral) implied volatility (RMSE actual value in parenthesis). $\rho_{SX}^{i,VG}$: pairwise correlation coefficient from Eq. (5) and the QF-based calibrated parameters. $\rho_{SX}^{h,VG}$: recovered pairwise historical correlation. s, κ: indices of skewness and excess kurtosis as in Cont and Tankov (2004). Data: see Tables 2 and B.3.

	QF-based calibration				HC-based calibration			
	Idiosyncratic process		Systematic process			Idiosyncratic process		Systematic process	
	USDJPY	Nikkei 225				USDJPY	Nikkei 225		
θ_Y	0.1514	−0.0177	θ_Z	−0.1830	θ_Y	-0.1362	−0.3825	θ_Z	0.5978
σ_Y	0.0070	0.0150	σ_Z	0.1095	σ_Y	0.0294	0.1661	σ_Z	0.0956
κ_Y	0.0449	0.0084	κ_Z	0.0522	κ_Y	0.0456	0.0750	κ_Z	0.0307
a	0.4008	1.8110			a	0.2776	0.6158		
RMSE	1.66%	0.47%	(0.0009)		RMSE	1.29%	0.36%	(0.0007)	
$\rho_{SX}^{i,VG}$		0.8177			$\rho_{SX}^{h,VG}$		0.28		
	Margin process		Systematic process			Margin process		Systematic process	
	USDJPY	Nikkei 225				USDJPY	Nikkei 225		
$\mathbb{E}L(1)$	0.0781	−0.3491	$\mathbb{E}Z(1)$	−0.1830	$\mathbb{E}L(1)$	0.0297	−0.0144	$\mathbb{E}Z(1)$	0.5978
$\sqrt{\mathbb{V}arL(1)}$	0.0573	0.2129	$\sqrt{\mathbb{V}arZ(1)}$	0.1172	$\sqrt{\mathbb{V}arL(1)}$	0.0571	0.2149	$\sqrt{\mathbb{V}arZ(1)}$	0.1418
$s(L(1))$	−0.0495	−0.2324	$s(Z(1))$	−0.2341	$s(L(1))$	−0.0393	−0.2814	$s(Z(1))$	0.3173
$\kappa(L(1))$	0.1165	0.1920	$\kappa(Z(1))$	0.1940	$\kappa(L(1))$	0.1030	0.2379	$\kappa(Z(1))$	0.1649

Table 6

Top panel – calibrated parameters of the multivariate VG model. QF-based calibration: Z, a_S, a_X calibrated using Quanto futures quotes. HC-based calibration: Z, a_S, a_X calibrated using historical correlation (128 days). Bottom panel – moments of the resulting margin distribution. RMSE: percentage of the ATM (Delta neutral) implied volatility (RMSE actual value in parenthesis). $\rho_{SX}^{i,VG}$: pairwise correlation coefficient from Eq. (5) and the QF-based calibrated parameters. $\rho_{SX}^{h,VG}$: recovered pairwise historical correlation. s, κ: indices of skewness and excess kurtosis as in Cont and Tankov (2004). Data: see Tables 2 and B.4.

	QF-based calibration				HC-based calibration			
	Idiosyncratic process		Systematic process			Idiosyncratic process		Systematic process	
	ZARUSD	BRENT				ZARUSD	BRENT		
θ_Y	−0.2879	−0.3608	θ_Z	−0.2089	θ_Y	−0.3136	−0.4426	θ_Z	−0.3741
σ_Y	0.1436	0.1300	σ_Z	0.3446	σ_Y	0.1433	0.1289	σ_Z	0.3553
κ_Y	0.1208	0.9995	κ_Z	0.1525	κ_Y	0.1121	0.7052	κ_Z	0.1420
a	−0.2976	−0.9733			a	−0.2636	−0.8478		
RMSE	1.25%	0.57%	(0.0024)		RMSE	1.12%	0.51%	(0.0021)	
$\rho_{SX}^{i,VG}$		0.3449			$\rho_{SX}^{h,VG}$		0.3137		
	Margin process		Systematic process			Margin process		Systematic process	
	ZARUSD	BRENT				ZARUSD	BRENT		
$\mathbb{E}L(1)$	−0.2257	−0.1575	$\mathbb{E}Z(1)$	−0.2089	$\mathbb{E}L(1)$	−0.2150	−0.1254	$\mathbb{E}Z(1)$	−0.3741
$\sqrt{\mathbb{V}arL(1)}$	0.2043	0.5156	$\sqrt{\mathbb{V}arZ(1)}$	0.3541	$\sqrt{\mathbb{V}arL(1)}$	0.2042	0.5097	$\sqrt{\mathbb{V}arZ(1)}$	0.3822
$s(L(1))$	−0.2976	−0.7390	$s(Z(1))$	−0.2651	$s(L(1))$	−0.2975	−0.6666	$s(Z(1))$	−0.3980
$\kappa(L(1))$	0.3378	1.9232	$\kappa(Z(1))$	0.5049	$\kappa(L(1))$	0.3352	1.5804	$\kappa(Z(1))$	0.5340

converted in strikes following the procedure described in Bossens, Rayée, Skantzos, and Deelstra (2010).

Tables 3 and 4 report the model parameters obtained by the joint calibration to FX triangle, i.e. the solution to the optimization problem stated in Eqs. (28) and (29). We denote this calibration procedure as 'TRIANGLE-based calibration'. In the tables we also report the main features of the calibrated distribution of the FX rates log-returns. Figs. 1 and 3 illustrate the resulting implied volatility smiles: the quality of the procedure is confirmed by the fact that the implied volatilities generated by the calibrated model are within the corresponding market bid and ask volatilities for both the main currency pairs and the inferred cross rate.

As to highlight the importance of using market consistent information on dependence (in this case as extracted from the currency triangle), we compare these results with the ones obtained under the assumption that the systematic component and the loading factors are anchored to the historical correlation in a way similar to the HC-based calibration procedure illustrated in Section 3.3.1. This would be necessary for example in absence of liquidly traded options on the inferred cross rate. The historical correlation between the FX log-rates is estimated using the sample correlation, denoted as $\rho_{Xm|l Xg|l}^{h}$, based on a sample size of 128 days – which is reported

in Table 2 (although in Section 3.3.1 the measure of linear dependence used is the historical covariance, for ease of exposition in the remaining of the paper we convert this measurement into historical correlation).

Although the two calibration procedures generate very similar errors, as noted above, there is a noticeable discrepancy between the value of the implied correlation resulting from the calibration based on the triangles (38.6% and 72.2% respectively) and the historical estimate obtained using the sample correlation (45% and 56.7%, respectively). Further, when the parameters from the HC-based calibration are used to reproduce the smile of the inferred cross rate, the resulting curve violates the bounds given by the market bid and ask volatilities as illustrated in Figs. 2 and 4 – last panel on the right. This violation would inevitably imply a mispricing of options on the inferred cross-rate.

4.3. Quanto futures

4.3.1. Nikkei 225

We use market data from Bloomberg and the CME free web platform observed on June 13, 2014. Vanilla options on the Nikkei 225 index have maturity of 28 days (July 11, 2014) as these quotes
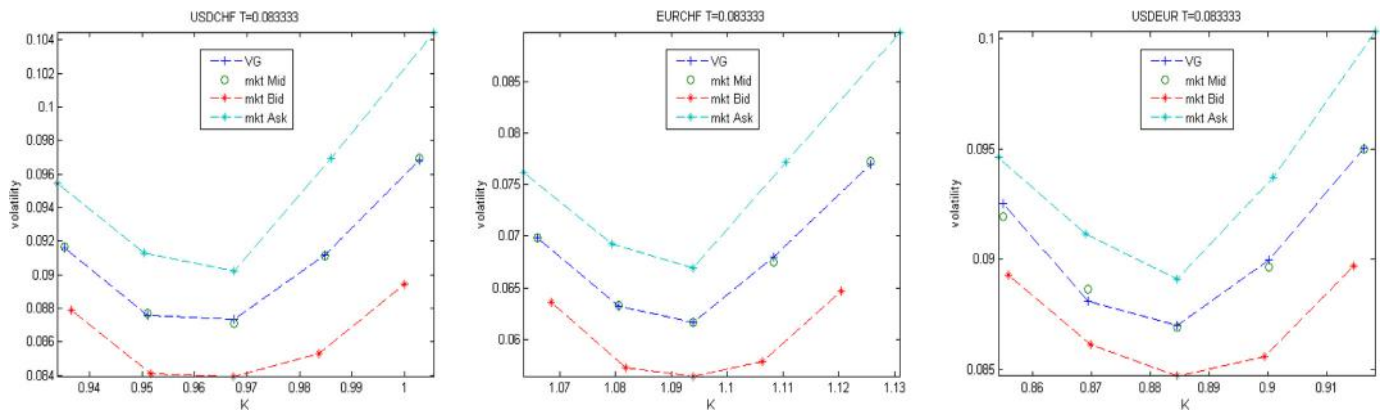
Fig. 1. USDCHF, EURCHF and USDEUR implied volatility in function of strike *K*: market vs. calibrated multivariate VG model. Options market data, March 17, 2016: Source: Bloomberg. Options maturity: *T* = 1 month. Market data: Tables 2 and B.1. Multivariate VG model parameters: Table 3, TRIANGLE-based calibration.
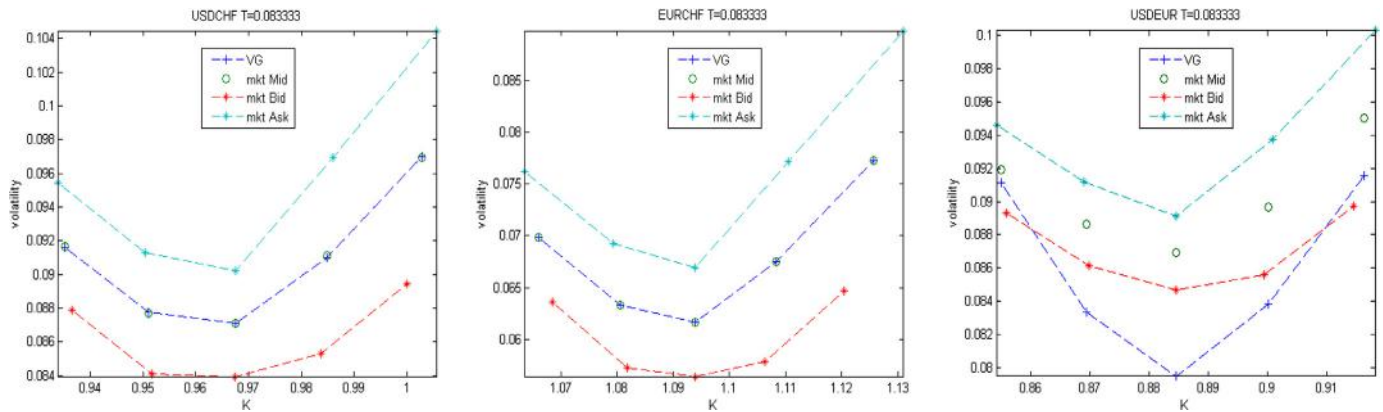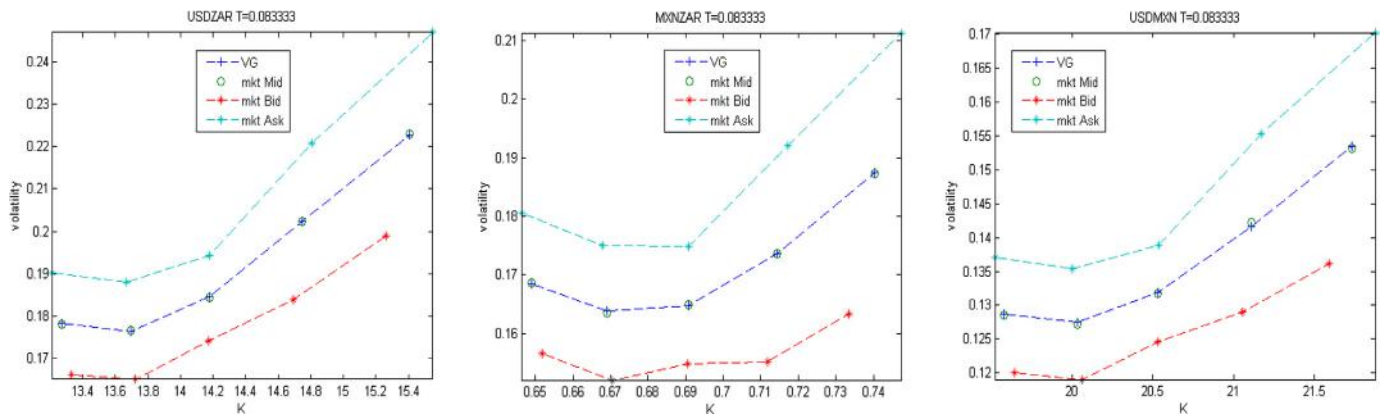

Fig. 2. USDCHF, EURCHF and USDEUR implied volatility in function of strike *K*: market vs. calibrated multivariate VG model. Options market data, March 17, 2016: Source: Bloomberg. Options maturity: *T* = 1 month. Market data: Tables 2 and B.1. Multivariate VG model parameters: Table 3, HC-based calibration.

Fig. 3. USDZAR, MXNZAR and USDMXN implied volatility in function of strike *K*: market vs. calibrated multivariate VG model. Options market data, December 21, 2016: Source: Bloomberg. Options maturity: *T* = 1 month. Market data: Tables 2 and B.2. Multivariate VG model parameters: Table 4, TRIANGLE-based calibration.

were the most liquid in the market[2]; consequently, we have chosen vanilla options on the USDJPY FX rate with similar maturity, regardless of the fact that the FX market shows high liquidity across other maturities as well. In particular, we consider 9 different strikes for the Nikkei 225 index options and 5 different strikes for the USDJPY exchange rate options. The futures contracts considered have a maturity in 91 days (September 12, 2014); similarly

to the previous section, the historical correlation between the log-returns of the Nikkei 225 index and the USDJPY FX rate is estimated using the sample correlation, denoted as ρ_{SX}^h, based on a sample size of 128 days. We just notice that the quotes of the Nikkei 225 index rates are end-of-day quotes, whereas the other quotes were observed at 3 p.m. GMT.

Results are summarized in Table 5, in which we report the model parameters obtained from the two alternative calibration procedures, i.e. the QF-based calibration given by the optimization problem in Eqs. (35), (38), (39) and the HC-based calibration given by the optimization problem in Eq. (42) (and (38)–(39)). Fig. 5 shows the market volatility smile and the calibrated one

---

[2] Options with maturity of 56 days (August 8, 2014) were also available but with limited liquidity. A set of options with various maturities were quoted by Bloomberg but without trading volume. Prices for these maturities are obtained from Bloomberg models and can therefore not be considered as market prices.
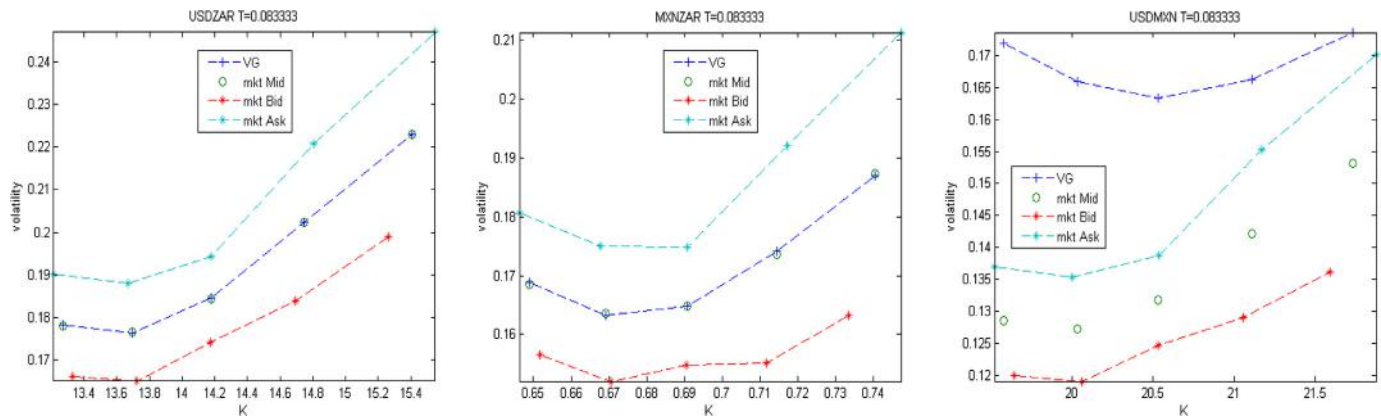
Fig. 4. USDZAR, MXNZAR and USDMXN implied volatility in function of strike K: market vs. calibrated multivariate VG model. Options market data, December 21, 2016: Source: Bloomberg. Options maturity: $T = 1$ month. Market data: Tables 2 and B.2. Multivariate VG model parameters: Table 4, HC-based calibration.
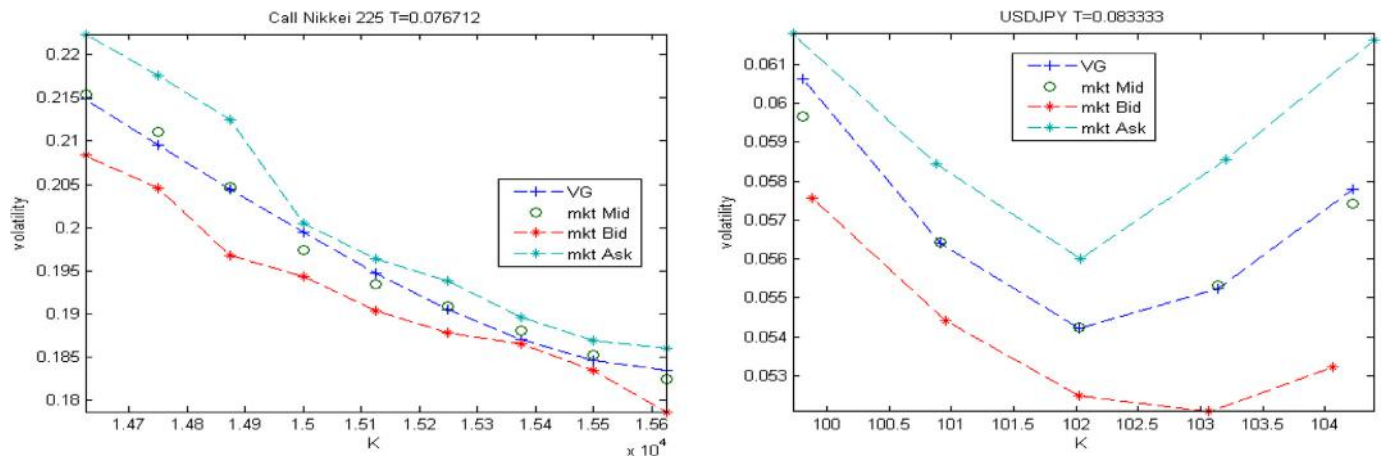

Fig. 5. USDJPY and Nikkei 225 implied volatility in function of strike K: market vs. calibrated multivariate VG model. Options market data, June 13, 2014: Source: Bloomberg. USDJPY Options maturity: $T = 1$ month. Nikkei 225 Options maturity: $T = 28$ days (July 11, 2014). Market data: Tables 2 and B.3. Multivariate VG model parameters: Table 5, QF-based calibration.

originated by our multivariate VG model for both Nikkei 225 and USDJPY vanilla options with parameters from the QF-based calibration (similar results are obtained under the HC-based calibration and are available upon request). In particular, the implied volatilities generated by the calibrated multivariate VG model are always bounded by the corresponding market bid and ask volatilities under both calibration assumptions.

In more details, from Table 5 we observe that, although both procedures are highly accurate, the calibrated parameters generate distributions of the margin processes for the log-returns of the Nikkei 225 index and the USDJPY FX rate which are relatively different under the two calibration assumptions. The assets log-return distributions, in fact, are characterized by very similar volatility (meant as the square root of the process' variance), however the Nikkei 225 index one shows a more pronounced left skew with thicker tails under the HC-based calibration, whilst the USDJPY FX rate distribution presents these features under the QF-based calibration. We also note that the skewness of the distribution of systematic risk process $Z(t)$ changes sign from one calibration procedure to the other.

Finally, Table 5 reports the pairwise linear correlation coefficient between the log-returns of the Nikkei 225 index and the USDJPY spot FX rate computed on the basis of these calibrated parameters and Eq. (5). We note the significant difference between the correlation coefficient implied by the QF-based calibration, $\rho_{SX}^{i,VG}$, which returns a value of 81.77%, and the correlation generated by the HC-based calibration, $\rho_{SX}^{h,VG}$, which matches

exactly the given 128-day historical correlation value at 28%. For comparison purposes, the historical correlation computed using a sample of 1 year daily data is 37.7%, and 39.72% if a sample of 2 years daily data is considered instead. Similar discrepancies are observed when both calibration procedures are repeated overtime (see Appendix C). With hindsight, a possible motivation for the observed differences could be traced back to the unprecedented monetary easing policies implemented by the Japanese government aimed at ending deflation. From this simple analysis it transpires that the market was already anticipating in June 2014 the impact of these monetary policies. Admittedly, 8 months later, in February 2015, the Nikkei Stock Average rose to a 15 years high, whilst the Yen settled around the weakest level against the US Dollar since 2007.

4.3.2. Brent crude oil

We use market data from Bloomberg observed on April 15, 2016. In particular, we use liquid market quotes of vanilla options on the Brent futures (expiring on August 11, 2016) with maturity of 73 days (June 27, 2016). Furthermore, we observe vanilla options on the ZARUSD FX rate with similar maturity. We consider 20 different strikes for the options on the Brent futures and 5 different strikes for the ZARUSD exchange rate options. For the QF-based calibration – given by the optimization problem in Eqs. (35), (38) and (39) – we use the two futures quotes available, namely with maturity May 10 and August 11, 2016. For the HC-based calibration – optimization problem in Eq. (42) (and (38)–(39)) – we
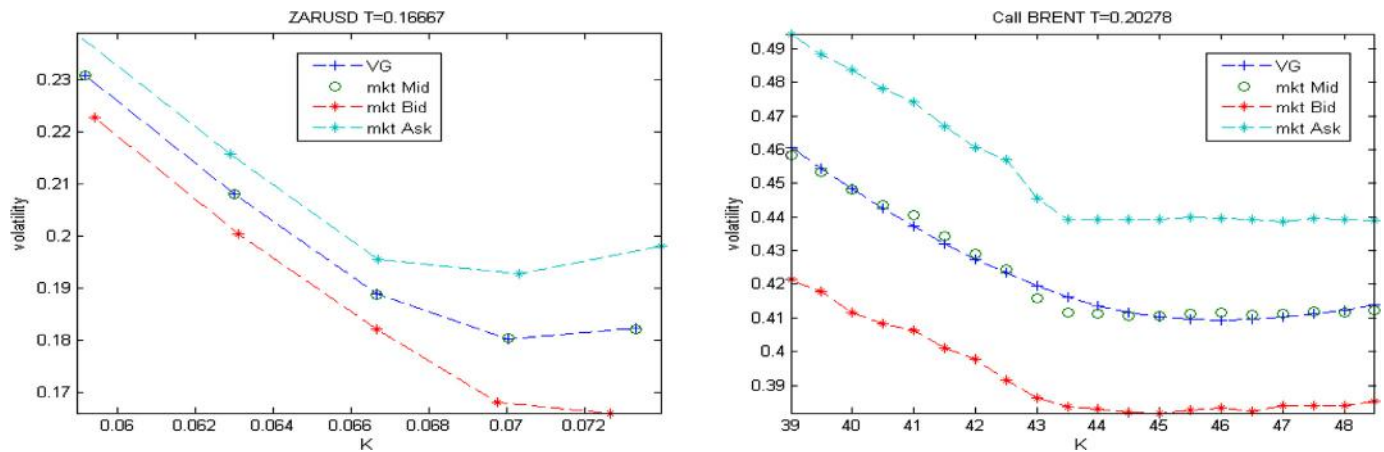
Fig. 6. ZARUSD and BRENT implied volatility in function of strike K: market vs. calibrated multivariate VG model. Options market data, April 15, 2016: Source: Bloomberg. ZARUSD Options maturity: $T = 2$ month. BRENT Options maturity: $T = 73$ days. Market data: Tables 2 and B.4. Multivariate VG model parameters: Table 6, QF-based calibration.

estimate the historical correlation between the log-returns of the Brent and the ZARUSD FX rate using the sample correlation based on a sample size of 128 days.

Results from both calibration procedures are summarized in Table 6; the goodness of fit is shown in Fig. 6: also in this example the recovered implied volatility smile is within the market bid-ask spread regardless of the calibration procedure used. Similarly to the previous cases, the QF-based and HC-based calibrations originate different values of the correlation indices, which are reported in Table 6, although in this instance the discrepancy is relatively minimal, 34.6% to 31.4%. We also observe that the relevant distribution features are quite similar under both calibration assumptions.

4.4. Implied correlation from Quanto options

In this section, we aim at further testing the consistency of the two calibration procedures on Quanto futures introduced in Section 3.3.1 and performed in Section 4.3 through the pricing of Quanto options. As discussed in Section 3.3.2, due to the fact that in our framework these products can be easily priced via analytical formulas (up to a Fourier inversion), these prices can be used to back out the relevant correlation. However, although market quotes for Quanto options are available from the CME platform, we do not have access to them and therefore we base our analysis on model prices obtained using the parameters recovered from both calibration procedures. Then, we can recover the value of the correlation coefficient such that the computed Quanto call option prices are matched by the ones obtained in the Black–Scholes model. To this purpose, though, we need first to carefully deal with the volatility smile/skew effect. Common market practice is, in fact, to use the at-the-money implied volatility; pricing of multi-asset options, such as Quanto options, though requires consistency with the volatility smile of the corresponding assets (see also Shevchenko, 2006). This is evident when we use Eq. (43) with $Q_{adj} = 1$ in the Black–Scholes setting to recover the correlation coefficient value such that the Quanto call prices generated by the multivariate VG model are matched exactly.

We focus in particular on the case of the Nikkei 225 index, due to the large discrepancies observed in Section 4.3.1. Results are presented in Fig. 7, in which we show the implied correlation coefficient extracted from the Black–Scholes model under the assumption that the volatility of both the Nikkei 225 index and the USDJPY FX rate is set at the corresponding at-the-money value, and under the assumption that the volatility smile of the index is in-

corporated in the procedure. In details, in the left hand side panel of Fig. 7, we illustrate the case in which the input Quanto option prices are generated using the parameters from the QF-based calibration; we denote the resulting implied correlation coefficients as $\rho_{SX}^{i,BS}(K; \nu_1)$ if at-the-money volatilities are used, and $\rho_{SX}^{i,BS}(K; \nu_2)$ if the whole volatility smile is incorporated instead. Similarly, in the right hand side panel of Fig. 7 we report the same quantities obtained from input prices generated by the parameters from the HC-based calibration; we denote these coefficients as $\rho_{SX}^{h,BS}(K; \nu_1)$ and $\rho_{SX}^{h,BS}(K; \nu_2)$. We note that when input prices are generated with at-the-money volatilities, implied correlation values are close to their admissible bounds $[-1, 1]$ regardless of the calibration approach adopted; this in turn generates a pronounced mispricing of in-the-money and out-of-the-money options (results available upon request). If instead the volatility smile is used, the resulting implied correlation values show an increasing pattern from 70.91% to 79.54% in the case of input parameters obtained from the QF-based calibration, and 34.74% to 52.76% in the case of input parameters from the HC-based calibration. This shows a mild correlation skew pattern.

However, from this simple experiment, we observe that once the volatility smile of the underlying asset is correctly taken into account, information extracted from historical prices generates inconsistent estimates of the correlation value; by using the parameters obtained from the HC-based calibration, in fact, we would expect to recover – compatibly with correlation skew patterns – values of the correlation close to the historical estimate of 28% used in the calibration. This procedure instead generates a discrepancy in the correlation value ranging from 58% to 88%. The parameters obtained from the QF-based calibration, on the other hand, generate values of the correlation relatively close to the one originated by the Quanto futures quotes, as the (percentage) difference ranges from 3% to 13%.

Similar considerations hold for the case of the Brent Crude Oil index; although for this particular data set the correlation skew effect is much stronger, in that the implied correlation ranges from 49.72% (for ITM Quanto call options) to 68.52% (for OTM Quanto call options), the values of the correlation recovered from the HC-based calibration produce larger discrepancies (in the interest of space we omit the results which are available upon request).

4.5. Tail dependence and risk measures

Proposition 3 shows that in our multivariate Lévy framework, the tail dependence behavior is governed by the tail probabilities
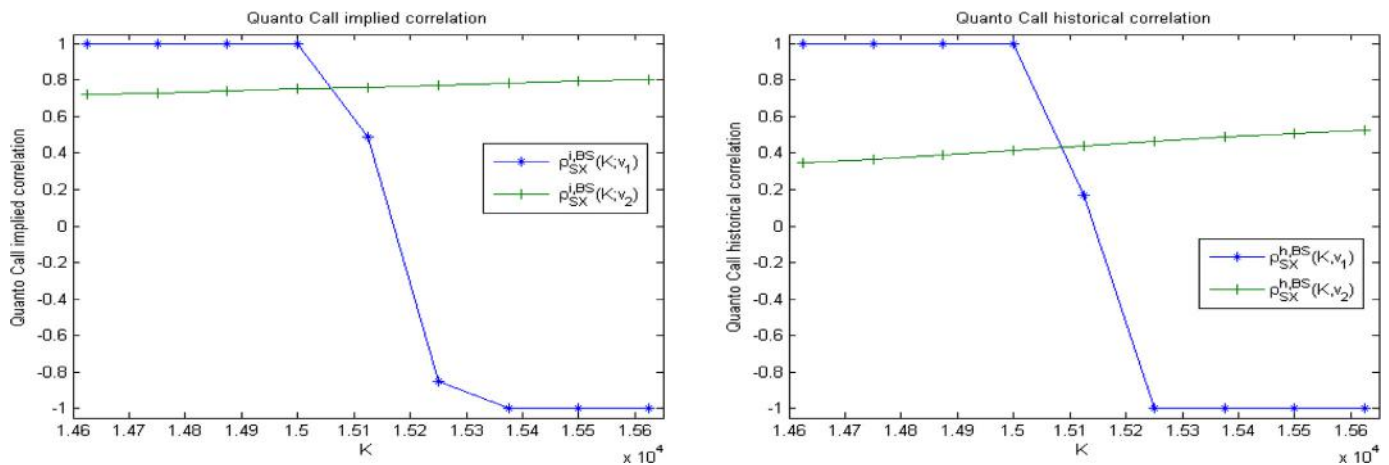
Fig. 7. Left hand panel: QF-based calibration. Right hand panel: HC-based calibration. $\rho_{SX}^{i,BS}(K; v_1)$: Quanto call implied correlation in function of strike K, extracted in a BS setting where the Nikkei 225 index and the USDJPY FX rate volatility are set at their at-the-money values (see Table B.3). $\rho_{SX}^{i,BS}(K; v_2)$: Quanto call implied correlation in function of strike K, extracted in a BS setting where the strike corresponding Nikkei 225 index implied volatility (Fig. 5) is used. Market data: see Tables 2 and B.3.
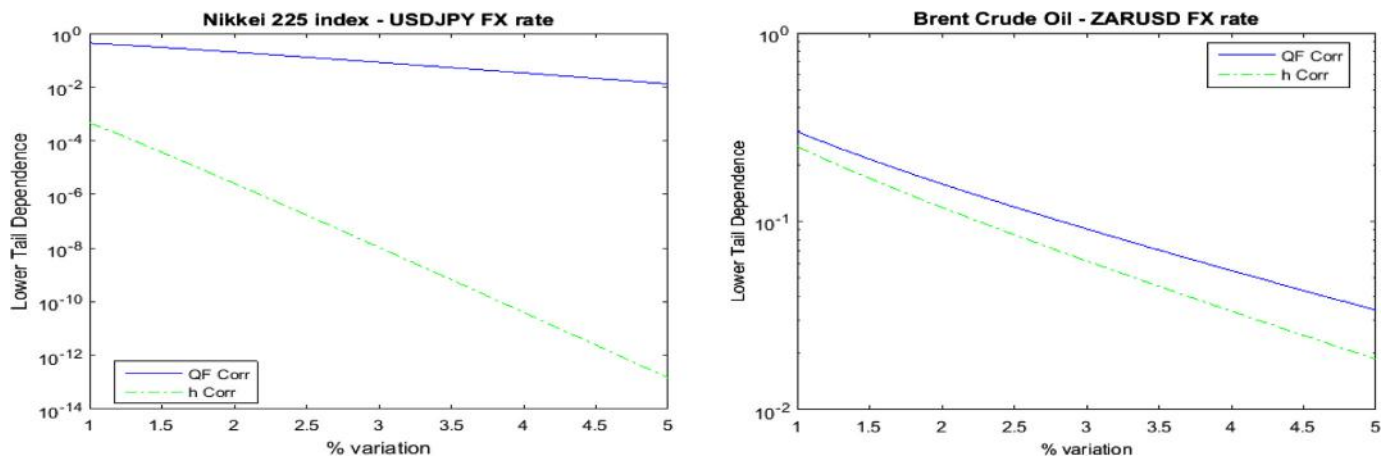

Fig. 8. Lower tail dependence for given percentage variations of the log-returns (on a log-scale). QF Corr: QF-based calibration. *h* Corr: HC-based calibration. Parameters: Tables 5 and 6.

of the systematic risk process *Z*, and the indices of upper/lower tail dependence are different from zero only when the margin processes are positively correlated, which is the case in the examples discussed in the previous sections. Hence, we use Eqs. (6) and (7), derived in Section 2 to compute the indices of lower tail dependence for the case of both Nikkei 225 index/USDJPY FX rate and Brent Crude Oil index/ZARUSD FX rate using the calibrated multivariate VG model; corresponding analytical expressions are recovered following a similar argument as in Barndorff-Nielsen and Shiryaev (2010)[3]. We consider a 1 week horizon; also we use the parameters obtained from both calibration procedures provided in Sections 4.3.1 and 4.3.2. Results are shown in Fig. 8, from which we note that both calibrated VG models produce a non negligible tail dependence effect. Specifically, in light of the previous discussion, we observe that correlated downwards jumps are more likely according to the prevailing market expectations than what experienced in the past, as in both cases the index of lower tail dependence is significantly higher when the parameters of the systematic risk process are recovered from Quanto futures. Although this is more evident for the case of the Nikkei 225 index/USDJPY FX rate (left hand side panel of Fig. 8), for which we noticed the significant difference in the values of the recovered correlation as discussed in Section 4.3.1, this effect is also noticeable in the case of the Brent Crude Oil index/ZARUSD FX rate (right hand side panel

of Fig. 8), in spite of the minimal discrepancy in the correlation values discussed in Section 4.3.2. In other words, although information from historical prices might lead to similar values of the correlation, i.e. linear dependence, as the ones implied by suitable market instruments, the same information can nevertheless cause a significant underestimation of the probability of a joint downward movement; this effect could have an impact on potential capital requirements linked to this measure of risk.

The two alternative correlation assumptions underpinning the calibration approaches discussed in this section also have an influence on univariate contracts. This is evident, for example, in the computation of the Value-at-Risk (VaR) of positions in non linear contracts, as vanilla call options, defined as the potential loss given a prespecified level of probability due to market movements. We illustrate the point by computing the 95% VaR for a short position in one call option on both indices, i.e. Nikkei 225 and Brent Crude Oil, over a 10 days exposure period (this example is inspired by Eberlein, Keller, & Prause, 1998). Results are presented in Fig. 9, which shows that the 95% VaR is higher under the QF-implied calibration procedure than under the historical calibration in both cases. Similarly to the case of joint downward risk, this shows that information extracted from historical prices could lead to underestimating the risk of losses for sell side market participants, again with cascading effects on potential capital requirements linked to these positions. Similar results can be obtained for alternative levels of confidence.

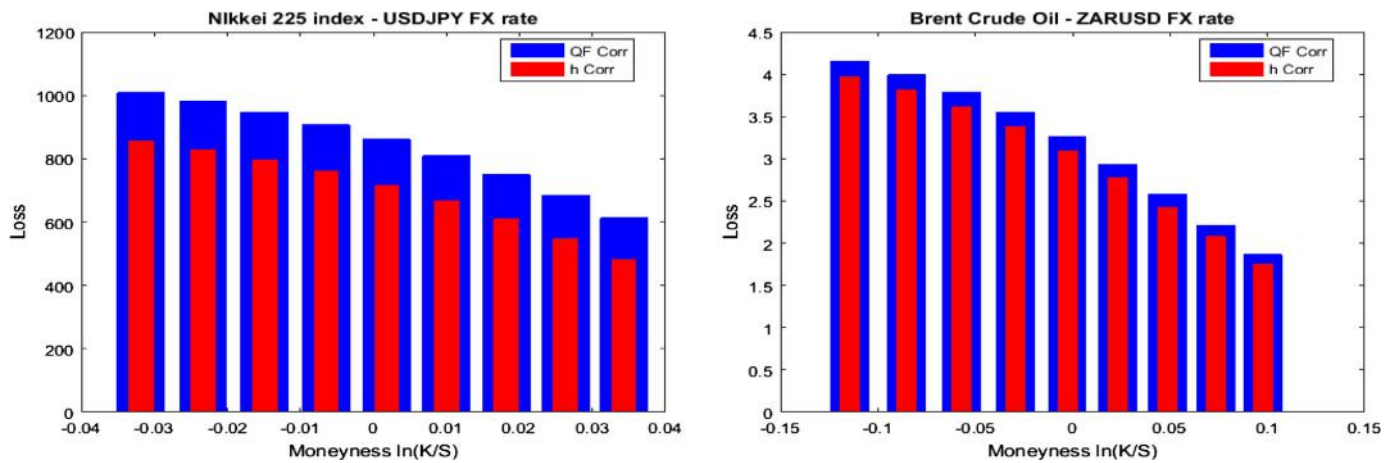[3] Formulas are available from the authors upon request.

Fig. 9. 95% VaR for a short call position – 10 days horizon. Option prices computed using the Carr–Madan method. QF Corr: QF-based calibration. *h* Corr: HC-based calibration. Parameters: Tables 5 and 6.

5. Conclusion

In this paper, we have developed a multivariate Lévy model for the joint dynamics of FX exchange rates and asset prices based on a factor representation of the margin risk process. In this setting, we consider the pricing and calibration of FX options and Quanto contracts of vanilla nature which are traded over-the-counter in significant size. The proposed model is general as it applies to any class of Lévy process with closed form expression for the characteristic exponent, it is also analytically tractable and provides access to a market consistent quantification of the dependence in place.

We conduct a numerical analysis on a number of sets of real market quotes. In particular, results show that the correlation implied by the considered products can be quite different from the historical correlation. This might have a significant impact on the indices of upper and lower tail dependence and on the computation of risk measures related to portfolios containing these products: information based on historical correlation leads to underestimating both the probability of a joint downward movement in the relevant assets, and the VaR of short positions in the derivative contracts under consideration.

As the proposed model is based on Lévy processes, i.e. processes with independent and stationary increments, stochastic volatility effects are ignored. For the case of the analysis considered in this paper, this is acceptable due to the very short maturities of the contracts involved. However, it is shown in the literature that stochastic volatility effects can be added by means of time changes (see Carr and Wu, 2007, for example); the extension to the multidimensional case is though subject of current research. Further research concerning applications of the model proposed in this paper could be the analysis of model risk, with respect to the distributions corresponding to the processes indicated in Table 1, in the context of capturing the joint dynamics of FX rates and other securities, as well as pricing multinames FX derivative contracts in the spirit of Barrieu and Scandolo (2015), Coqueret and Tavin (2016).

Appendix A. Proofs of results

A1. Proof of Proposition 1

Let $\mathbf{a} = (a_1, \ldots, a_n)^\top$, and assume that $\mathbf{\Lambda}(t)$ has generating triplet (β, Γ, ν). It follows from Sato (1999, E12.10) (see also Cont and Tankov, 2004, Proposition 5.3) that $\beta = (\beta_1, \ldots, \beta_n, \beta_Z)^\top$, Γ is diagonal and ν is supported by the union of the coordinate axes. Define a $n \times (n+1)$ matrix M as

$$M = \begin{bmatrix} 1 & 0 & \ldots & 0 & a_1 \\ 0 & 1 & \ldots & 0 & a_2 \\ \vdots & \vdots & \ldots & \vdots & \vdots \\ 0 & 0 & \ldots & 1 & a_n \end{bmatrix}.$$

Then $\mathbf{L}(t) = M\mathbf{\Lambda}(t)$; it follows from Sato (1999, Proposition 11.10) (see also Cont and Tankov, 2004, Theorem 4.1) that $\mathbf{L}(t)$ is a Lévy process with drift and diffusion matrix as given. The characteristic function follows from the independence of the components of $\mathbf{\Lambda}(t)$. For the construction of the Lévy measure, we note that $\{\mathbf{a}\Delta Z(t) \neq 0, \mathbf{a}\Delta Z(t) \in B\}$ if and only if $\{\Delta Z(t) \neq 0, \Delta Z(t) \in A\}$. As the components of $\mathbf{\Lambda}(t)$ are independent, Sato (1999, E12.10) implies that the support of κ is the union of the coordinate axes and the result follows. See Tankov (2004) as well.

A2. Proof of Corollary 2

Results for γ_{Lj}, c_j^2 follow from Cont and Tankov (2004, Proposition 5.2); the Lévy measure follows from Cont and Tankov (2004, Proposition 5.3) and Sato (1999, E12.10) by recognizing that $L_j(t) = Y_j(t) + a_j Z(t)$ and $Y_j(t)$ is independent of $Z(t)$.

A3. Proof of Proposition 3

The proof of the results of Proposition 3 is based on the fact that the probability of two sums of variables both exceeding some diverging threshold is driven completely by the common component of the sums (see Oh and Patton, 2012, for example).

(a) Applying the above, we obtain

$$\mathbb{P}\big(L_j(t) < l_j, L_k(t) < l_k\big)$$
$$= \mathbb{P}\big(Y_j(t) + a_j Z(t) < l_j, Y_k(t) + a_k Z(t) < l_k\big)$$
$$\simeq \mathbb{P}\big(a_j Z(t) < l_j, a_k Z(t) < l_k\big) \quad l_j, l_k \downarrow -\infty.$$

Hence, if $a_j, a_k > 0$

$$\mathbb{P}\big(L_j(t) < l_j, L_k(t) < l_k\big)$$
$$\simeq \mathbb{P}\left(Z(t) < \min\left\{\frac{l_j}{a_j}, \frac{l_k}{a_k}\right\}\right) \quad l_j, l_k \downarrow -\infty,$$

whilst, if $a_j, a_k < 0$

$$\mathbb{P}\big(L_j(t) < l_j, L_k(t) < l_k\big)$$
$$\simeq \mathbb{P}\left(Z(t) > \max\left\{\left|\frac{l_j}{a_j}\right|, \left|\frac{l_k}{a_k}\right|\right\}\right) \quad l_j, l_k \downarrow -\infty.$$

On the other hand, if $\rho_{jk}^{\mathbf{L}} < 0$ for all $t > 0$, we obtain

$$\mathbb{P}\big(L_j(t) < l_j, L_k(t) < l_k\big)$$
$$\simeq \mathbb{P}\left(Z(t) > \left|\frac{l_j}{a_j}\right|, Z(t) < \frac{l_k}{a_k}\right) \quad l_j, l_k \downarrow -\infty$$

if $a_j < 0 < a_k$, and

$$\mathbb{P}\big(L_j(t) < l_j, L_k(t) < l_k\big)$$
$$\simeq \mathbb{P}\left(Z(t) < \frac{l_j}{a_j}, Z(t) > \left|\frac{l_k}{a_k}\right|\right) \quad l_j, l_k \downarrow -\infty$$

if $a_k < 0 < a_j$; therefore both probabilities are equal to zero.
(b) The result follows by the same argument as above.

A4. Proof of Proposition 4

The Girsanov theorem (see Barndorff-Nielsen and Shiryaev, 2010, for example) implies that the change of measure is in this case governed by the Esscher parameter $h_j \in \mathbb{R}$, which is constant by construction. Consequently the processes $\mathbf{\Lambda}(t)$ and $\mathbf{L}(t)$ remain Lévy processes under $\mathbb{P}^{hj}$. Therefore, the Girsanov theorem implies that the triplets of the process $\mathbf{L}(t)$ under $\mathbb{P}^{hj}$ are

$$L_j(t) : \left(\gamma_{Lj} + h_j c_j^2 + \int_{\mathbb{R}} x(e^{h_j x} - 1)\kappa_j(dx), c_j^2, e^{h_j x}\kappa_j\right)$$
$$L_k(t) : \left(\gamma_{Lk} + h_j a_j a_k \sigma_Z^2 + a_k \int_{\mathbb{R}} z(e^{h_j a_j z} - 1)\nu_Z(dz), c_k^2, \nu_k + e^{h_j a_j z}\nu_Z\right),$$
$$k \neq j, k = 1, \cdots, n.$$

Proposition 1 and Corollary 2 give the required result. See also Eberlein et al. (2009).

A5. Proof of Proposition 5

(a) By construction, under $\mathbb{P}^l$, we have

$$X^{l|m}(t) = X^{l|m}(0)$$
$$\times e^{(r_m - r_l + \varphi_{Y_{X_{m|l}}}^l(-i) + \varphi_Z^l(-ia_{X_{m|l}}))t - Y_{X_{m|l}}(t) - a_{X_{m|l}}Z(t)}.$$

Set $Y_{X_{l|m}}(t) = -Y_{X_{m|l}}(t)$; then $Y_{X_{l|m}}(t)$ is a Lévy process due to invariance under linear transformation and its characteristic exponent is $\varphi_{Y_{X_{l|m}}}(u) = \varphi_{Y_{X_{m|l}}}(-u)$. Also, $Y_{X_{l|m}}$ is independent of $Z(t)$. Further, notice that $\varphi_{Y_{X_{m|l}}}^l(-i) = -\varphi_{Y_{X_{l|m}}}^m(-i)$ and $\varphi_Z^l(-ia_{X_{m|l}}) = -\varphi_Z^m(-ia_{X_{l|m}})$. The invariance under the Esscher change of measure and Proposition 4 imply the result.
(b) By construction, under $\mathbb{P}^l$, we have

$$X^{m|g}(t) = X^{m|g}(0)e^{(r_g - r_m - \varphi_{Y_{X_{m|l}}}^l(-i) - \varphi_Z^l(-ia_{X_{m|l}}) + \varphi_{Y_{X_{g|l}}}^l(-i) + \varphi_Z^l(-ia_{X_{g|l}}))t + Y_{X_{m|l}}(t) - Y_{X_{g|l}}(t) + \left(a_{X_{m|l}} - a_{X_{g|l}}\right)Z(t)}.$$

Set $Y_{X_{m|g}}(t) = Y_{X_{m|l}}(t) - Y_{X_{g|l}}(t)$; then $Y_{X_{m|g}}(t)$ is a Lévy process due to invariance under linear transformation and its characteristic exponent is $\varphi_{Y_{X_{m|g}}}(u) = \varphi_{Y_{X_{m|l}}}(u) + \varphi_{Y_{X_{g|l}}}(-u)$. Also, $Y_{X_{m|g}}(t)$ is independent of $Z(t)$. Further, notice that $\varphi_{Y_{X_{g|l}}}^l(-i) = -\varphi_{Y_{X_{g|l}}}^g(i)$ and $-\varphi_Z^l(-ia_{X_{m|l}}) + \varphi_Z^l(-ia_{X_{g|l}}) = -\varphi_Z^g(-i(a_{X_{m|l}} - a_{X_{g|l}}))$. Then, Proposition 4 implies that $Y_{X_{m|l}}(t)$ is unaffected by the change of measure as it is independent of $Y_{X_{g|l}}(t)$ and $Z(t)$; further $Y_{X_{g|l}}(t)$ and $Z(t)$ remain Lévy processes, and their linear combination is therefore a Lévy process. Eqs. (18)–(20) follow from Proposition 4.

We note that Theorem 4.1 and Proposition 5.3 in Cont and Tankov (2004) imply that the process $Y_{X_{m|g}}(t)$ has triplet $(\sigma_{X_{g|l}}^2 + \int_{\mathbb{R}} y(e^y - 1)\nu_{X_{g|l}}(dy), \sigma_{X_{m|g}}^2 = \sigma_{X_{m|l}}^2 + \sigma_{X_{g|l}}^2, \nu_{X_{m|l}} + e^y \nu_{X_{g|l}})$.

Appendix B. Market implied volatilities

Table B.1
USDCHF, EURCHF and USDEUR implied volatility. σ_{mkt}: market mid implied volatility – the value in the third column denotes the so-called At-The-Money (ATM) Delta neutral implied volatility; σ_{VG}^i: VG implied volatility from TRIANGLE-based calibration; σ_{VG}^h: VG implied volatility from HC-based calibration.

	USDCHF				
K	0.9352	0.9511	0.9675	0.9848	1.0029
σ_{mkt}	0.0917	0.0877	0.0871	0.0911	0.0970
σ_{VG}^i	0.0916	0.0876	0.0874	0.0912	0.0968
σ_{VG}^h	0.0916	0.0878	0.0871	0.0910	0.0970
	EURCHF				
K	1.0660	1.0805	1.0939	1.1084	1.1257
σ_{mkt}	0.0699	0.0633	0.0617	0.0675	0.0772
σ_{VG}^i	0.0699	0.0632	0.0616	0.0680	0.0770
σ_{VG}^h	0.0699	0.0633	0.0617	0.0675	0.0772
	USDEUR				
K	0.8550	0.8694	0.8846	0.9002	0.9163
σ_{mkt}	0.092	0.089	0.087	0.090	0.095
σ_{VG}^i	0.093	0.088	0.087	0.090	0.095
σ_{VG}^h	0.091	0.083	0.079	0.084	0.092

Table B.2

USDZAR, MXNZAR and USDMXN implied volatility. σ_{mkt}: market mid implied volatility – the value in the third column denotes the so-called At-The-Money (ATM) Delta neutral implied volatility; σ_{VG}^{i}: VG implied volatility from TRIANGLE-based calibration; σ_{VG}^{h}: VG implied volatility from HC-based calibration.

	USDZAR				
K	13.2711	13.6958	14.1760	14.7495	15.4046
σ_{mkt}	0.1781	0.1765	0.1842	0.2024	0.2230
σ_{VG}^{i}	0.1783	0.1762	0.1846	0.2023	0.2229
σ_{VG}^{h}	0.1783	0.1763	0.1845	0.2023	0.2229
	MXNZAR				
K	0.6491	0.6692	0.6907	0.7144	0.7404
σ_{mkt}	0.1686	0.1636	0.1648	0.1736	0.1873
σ_{VG}^{i}	0.1686	0.1638	0.1647	0.1737	0.1874
σ_{VG}^{h}	0.1688	0.1632	0.1649	0.1741	0.1870
	USDMXN				
K	19.5794	20.0302	20.5331	21.1114	21.7357
σ_{mkt}	0.1285	0.1272	0.1317	0.1421	0.1532
σ_{VG}^{i}	0.1287	0.1275	0.1320	0.1417	0.1534
σ_{VG}^{h}	0.1719	0.1659	0.1633	0.1663	0.1736

Table B.3

USDJPY and Nikkei 225 implied volatility. σ_{mkt}: market mid implied volatility - the value in the third column denotes the so-called At-The-Money (ATM) Delta neutral implied volatility; σ_{VG}^{i}: VG implied volatility from QF-based calibration; σ_{VG}^{h}: VG implied volatility from HC-based calibration.

	USDJPY				
K	99.8047	100.9160	102.0298	103.1348	104.2219
σ_{mkt}	0.0597	0.0564	0.0543	0.0553	0.0574
σ_{VG}^{i}	0.0606	0.0564	0.0542	0.0552	0.0578
σ_{VG}^{h}	0.0600	0.0563	0.0543	0.0552	0.0576
	Nikkei 225				
K	14625	14875	15125	15375	15625
σ_{mkt}	0.2154	0.2046	0.1934	0.1880	0.1824
σ_{VG}^{i}	0.2149	0.2044	0.1946	0.1870	0.1835
σ_{VG}^{h}	0.2159	0.2043	0.1941	0.1870	0.1835

Table B.4

ZARUSD and BRENT implied volatility. σ_{mkt}: market mid implied volatility - the value in the third column denotes the so-called At-The-Money (ATM) Delta neutral implied volatility; σ_{VG}^{i}: VG implied volatility from QF-based calibration; σ_{VG}^{h}: VG implied volatility from HC-based calibration.

	ZARUSD				
K	0.0592	0.0630	0.0667	0.0700	0.0733
σ_{mkt}	0.2308	0.2080	0.1888	0.1805	0.1821
σ_{VG}^{i}	0.2308	0.2080	0.1890	0.1802	0.1823
σ_{VG}^{h}	0.2308	0.2080	0.1890	0.1803	0.1822
	BRENT				
K	39	41	43,5	46	48,5
σ_{mkt}	0.4584	0.4405	0.4115	0.4115	0.4122
σ_{VG}^{i}	0.4607	0.4372	0.4163	0.4093	0.4138
σ_{VG}^{h}	0.4610	0.4370	0.4161	0.4093	0.4136

Appendix C. Nikkei 225 Quanto futures: time analysis

To better study the behavior of the correlation coefficient, we repeat both the QF-based and HC-based calibration procedures every day from June 13, 2014 to June 20, 2014. Results are illustrated in Table C.1. Specifically, we report the market futures prices, F_{mkt}^{f}, the market and VG Quanto futures prices, F_{mkt}^{d} and F_{VG}^{d}, the at-the-money volatility of both Nikkei 225 index and USDJPY FX rate. The VG prices are obtained using the parameters from both calibration procedures. Further, we report the Quanto futures implied correlation obtained under both the multivariate VG model and the Black–Scholes framework (denoted as $\rho_{SX}^{i,VG}$, $\rho_{SX}^{i,BS}$ respectively) which are compared against the historical correlation; for completeness, we also consider the historical correlation coefficient computed over time periods of different lengths, spanning from 1 month to 2 years. These results show the dynamics over time of the relevant correlation coefficients. In particular we note that the historical correlation is relatively stable, but always fluctuates around a lower level than the implied one. The difference between these measures can be compared in a sense to the difference between implied volatility and historical volatilities. Many empirical studies show that implied and historical (including GARCH type) volatilities are quite different, as these measures provide different types of information: the implied volatility is a measure extracted from the market of derivatives and reflects market expectations (and as such it is highly dependent on market news and speculation), whilst the historical volatilities are backward-looking measures. Hence, the results from the calibration exercise show that the market expectation is for much stronger co-movements in the assets of interest (i.e. the Nikkei 225 index and the USDJPY exchange rate) than what experienced in the past.

Table C.1 also contains the market Quanto adjustments and the VG Quanto adjustment computed using the parameters obtained from both calibration procedures. Similarly, we report the resulting covariance between the log-returns of the Nikkei 225 index and USDJPY FX rate, which is computed day by day after calibration. Finally, the term corresponding to the cumulants of higher order than two of the jump part of the systematic risk factor in the Quanto adjustment is presented in the table as well, where we use the following notation:

$$qc_Z(n) = \sum_{k=1}^{n-1} \frac{a_S^{n-k} a_X^k}{k!(n-k)!} \int_{\mathbb{R}} z^n v_Z(dz), \qquad (C.1)$$

and

$$qc_Z(3) = \frac{a_S^2 a_X + a_S a_X^2}{2} \int_{\mathbb{R}} z^3 v_Z(dz), \qquad (C.2)$$

$$qc_Z(4) = \frac{2a_S^3 a_X + 3a_S^2 a_X^2 + 2a_S a_X^3}{12} \int_{\mathbb{R}} z^4 v_Z(dz). \qquad (C.3)$$

We note that the largest contribution to the overall Quanto adjustment originated by higher order cumulants is due to the skewness of the systematic factor Z, captured by the term $qc_Z(3)$ (see Eq. C.2), which fluctuates (in absolute value) between 0.22% and 3.51% for the case of the QF-based calibration. The contribution of the excess kurtosis term $qc_Z(4)$ (see Eq. C.3) counts for up to 0.21% of the overall Quanto adjustment, whilst the contribution of the higher order terms ($n > 4$) is negligible in comparison. Similar conclusions hold under the HC-based calibration, except for the fact that the contribution from the skewness term, $qc_Z(3)$, is relatively stable around 1%.

Table C.1

Time evolution analysis - $F_{mkt}^d(0,T)$: USD-denominated CME Nikkei 225 futures quote (symbol: NKD). $F_{mkt}^f(0,T)$: JPY-denominated CME Nikkei 225 futures quote (symbol: NIY). $F_{VG}^{d,i}(0,T)$: USD-denominated Nikkei 225 futures quote computed with equation (45)-(46) and QF-based calibration parameters. $F_{VG}^{d,h}(0,T)$: USD-denominated Nikkei 225 futures quote computed with equation (45)-(46) and HC-based calibration parameters. q_{mkt}: Quanto adjustment implied by market data. q_{VG}^i and $\mathbb{C}ov_{VG}^i(L_S, L_X)$: Quanto adjustment and covariance computed with QF-based calibration parameters. q_{VG}^h and $\mathbb{C}ov_{VG}^h(L_S, L_X)$: Quanto adjustment and covariance computed with HC-based calibration parameters. $qc_Z(3)$, $qc_Z(4)$ as in equations (C.2)-(C.3). Residual: $\sum_{n=5}^{\infty} qc_Z(n)$ - see equation (C.1).

	Friday 13/06/14	Monday 16/06/14	Tuesday 17/06/14	Wednesday 18/06/14	Thursday 19/06/14	Friday 20/06/14
T(days)	91	88	87	86	85	84
$F_{mkt}^f(0,T)$	15030.00	14950.00	15030.00	15100.00	15365.00	15460.00
$F_{mkt}^d(0,T)$	15065.00	14985.00	15060.00	15130.00	15390.00	15490.00
$F_{VG}^{d,i}(0,T)$	15066.37	14985.41	15059.95	15131.10	15388.83	15488.81
$F_{VG}^{d,h}(0,T)$	15043.15	14960.94	15042.08	15112.85	15374.77	15470.02
Nikkei 225 ATM vol	19.56%	18.14%	18.70%	17.04%	15.63%	18.36%
USDJPY ATM vol	5.42%	5.51%	5.42%	5.55%	4.98%	4.87%
$\rho_{SX}^{i,BS}$	87.90%	97.12%	82.59%	89.07%	89.60%	94.21%
$\rho_{SX}^{i,VG}$	81.77%	91.59%	74.27%	77.21%	77.95%	86.32%
ρ_h^{128d}	28.00%	28.78%	29.29%	30.45%	30.50%	29.81%
ρ_h^{2y}	39.72%	39.76%	39.76%	39.69%	39.63%	39.62%
ρ_h^{1y}	37.70%	39.39%	39.43%	39.58%	38.88%	40.04%
ρ_h^{6m}	29.39%	29.20%	28.51%	28.12%	27.78%	29.99%
ρ_h^{3m}	33.65%	34.35%	35.30%	33.31%	34.34%	29.99%
ρ_h^{1m}	43.15%	49.78%	50.93%	48.29%	43.67%	43.68%
q_{mkt}	9.33E-03	9.70E-03	8.37E-03	8.42E-03	6.98E-03	8.42E-03
q_{VG}^i	9.69E-03	9.81E-03	8.35E-03	8.73E-03	6.65E-03	8.09E-03
$\mathbb{C}ov_{VG}^i(L_S, L_X)$	9.98E-03	9.92E-03	8.63E-03	8.71E-03	6.70E-03	8.19E-03
$qc_Z^i(3)$	-3.03E-04	-1.13E-04	-2.93E-04	1.93E-05	-5.34E-05	-1.05E-04
$qc_Z^i(4)$	2.01E-05	5.52E-06	1.49E-05	4.69E-06	4.80E-06	1.45E-06
residual	-1.27E-06	-8.44E-08	-5.69E-07	1.76E-08	-5.23E-08	-1.86E-08
q_{VG}^h	3.51E-03	3.03E-03	3.37E-03	3.61E-03	2.73E-03	2.81E-03
$\mathbb{C}ov_{VG}^h(L_S, L_X)$	3.44E-03	3.07E-03	3.41E-03	3.57E-03	2.70E-03	2.84E-03
$qc_Z^h(3)$	6.91E-05	-3.26E-05	-4.57E-05	3.56E-05	2.66E-05	-3.06E-05
$qc_Z^h(4)$	1.35E-06	3.40E-07	5.63E-06	4.38E-07	2.52E-07	3.14E-07
residual	2.61E-08	-3.49E-09	-1.03E-07	4.83E-09	2.39E-09	-3.18E-09

References

Atanasov, V., & Nitschka, T. (2015). Foreign currency returns and systematic risks. *Journal of Financial and Quantitative Analysis, 50*, 231–250. http://dx.doi.org/10.1017/S002210901400043X.

Ballotta, L., & Bonfiglioli, E. (2016). Multivariate asset models using Lévy processes and applications. *The European Journal of Finance, 22*, 1320–1350. http://dx.doi.org/10.1080/1351847X.2013.870917.

Ballotta, L., & Fusai, G. (2015). Counterparty credit risk in a multivariate structural model with jumps. *Finance, Revue de l'Association Française de Finance, 36*, 39–74.

Barndorff-Nielsen, O. E. (1995). *Normal inverse Gaussian distributions and the modeling of stock returns*. Department of Theoretical Statistics, Aarhus University. Research report, 300.

Barndorff-Nielsen, O. E., & Shiryaev, A. (2010). Change of time and change of measure. Advanced series on statistical science and applied probability: 13. World Scientific.

Barrieu, P., & Scandolo, G. (2015). Assessing financial model risk. *European Journal of Operational Research, 242*, 546–556.

Basel (2010). *Basel III: A global regulatory framework for more resilient banks and banking systems*. http://www.bis.org/publ/bcbs189.pdf.

Bossens, F., Rayée, G., Skantzos, N. S., & Deelstra, G. (2010). Vanna-volga methods applied to FX derivatives: from theory to market practice. *International Journal of Theoretical and Applied Finance, 13*, 1293–1324.

Branger, N., & Muck, M. (2012). Keep on smiling? The pricing of Quanto options when all covariances are stochastic. *Journal of Banking & Finance, 36*, 1577–1591. http://dx.doi.org/10.1016/j.jbankfin.2012.01.004.

Carr, P., Geman, H., Madan, D. B., & Yor, M. (2002). The fine structure of asset returns: An empirical investigation. *Journal of Business, 75*, 305–332.

Carr, P., & Madan, D. B. (1999). Option valuation using the fast Fourier transform. *Journal of Computational Finance, 2*, 61–73.

Carr, P., & Wu, L. (2007). Stochastic skew in currency options. *Journal of Financial Economics, 86*, 213–247.

Chicago Board Options Exchange (2009). *CBOE S&P Implied Correlation Index*. http://www.cboe.com/micro/impliedcorrelation/ImpliedCorrelationIndicator.pdf.

Co, R., Kerpel, J., & Labuszewski, J. W. (2013). *Nikkei 225 spread opportunities*. CME Group. Technical report.

Cont, R., & Tankov, P. (2004). *Financial modelling with Jump Processes*. Chapman & Hall/CRC Press.

Coqueret, G., & Tavin, B. (2016). An investigation of model risk in a market with jumps and stochastic volatility. *European Journal of Operational Research, 253*, 648–658.

Da Fonseca, J., Grasselli, M., & Tebaldi, C. (2007). Option pricing when correlations are stochastic: an analytical framework. *Review of Derivative Research, 10*, 151–180.

De Col, A., Gnoatto, A., & Grasselli, M. (2013). Smiles all around: FX joint calibration in a multi-Heston model. *Journal of Banking & Finance, 37*, 3799–3818. http://dx.doi.org/10.1016/j.jbankfin.2013.05.031.

Eberlein, E. (2013). Fourier based valuation methods in mathematical finance. In F. Benth, V. Kholodnyi, & P. Laurence (Eds.), *Quantitative energy finance. modeling, pricing, and hedging in energy and commodity markets* (pp. 85–114). Springer.

Eberlein, E., Frey, R., & von Hammerstein, E. A. (2008). Advanced credit portfolio modeling and CDO pricing. . In W. Jäger, & H. Krebbs (Eds.), *Mathematics Key Technology for the Future* (pp. 253–279). Springer.

Eberlein, E., Keller, U., & Prause, K. (1998). New insights into smile, mispricing, and value at risk: The Hyperbolic model. *The Journal of Business, 71*, 371–405.

Eberlein, E., & Koval, N. (2006). A cross-currency Lévy market model. *Quantitative Finance, 6*, 465–480. http://dx.doi.org/10.1080/14697680600818791.

Eberlein, E., Papapantoleon, A., & Shiryaev, A. N. (2009). Esscher transform and the duality principle for multidimensional semimartingales. *The Annals of Applied Probability, 19*, 1944–1971. doi: 10.1214/09-AAP600.

Embrechts, P., McNeil, A., & Straumann, D. (2002). Correlation and dependence in risk management: properties and pitfalls. In M. Dempster (Ed.), *Risk management: Value at risk and beyond* (pp. 176–223). Cambridge University Press.

Fabozzi, F. J., Paletta, T., Stanescu, S., & Tunaru, R. (2016). An improved method for pricing and hedging long dated American options. *European Journal of Operational Research, 254*, 656–666.

Fang, F., & Oosterlee, C. (2009). Pricing early-exercise and discrete barrier options by fourier-cosine series expansions. *Numerische Mathematik, 114*, 27–62.

Geman, H., El Karoui, N., & Rochet, J. (1995). Changes of numéraire, changes of probability measure and option pricing. *Journal of Applied Probability, 32*, 443–458.

Gerber, H. U., & Shiu, E. S. W. (1994). Option pricing by Esscher transforms. *Transactions of Society of Actuaries, 46*, 99–140.

Giese, A. (2012). Quanto adjustments in the presence of stochastic volatility. *Risk, 25*, 67–71.

Itkin, A., & Lipton, A. (2015). Efficient solution of structural default models with correlated jumps and mutual obligations. *International Journal of Computer Mathematics, 92*, 2380–2405. http://dx.doi.org/10.1080/00207160.2015.1071360.

Lipton, A., & Sepp, A. (2009). Credit value adjustment for credit default swaps via the structural default model. *The Journal of Credit Risk, 5*, 127–150.

Lord, R., Fang, F., Bervoets, F., & Oosterlee, C. (2008). A fast and accurate FFT-based method for pricing early-exercise options under Lévy processes. *SIAM Journal on Scientific Computing, 30*, 1678–1705.

Luciano, E., Marena, M., & Semeraro, P. (2016). Dependence calibration and portfolio fit with factor-based time changes. *Quantitative Finance, 16*, 1037–1052.

Madan, D. B., Carr, P., & Chang, E. (1998). The Variance Gamma process and option pricing. *European Finance Review, 2*, 79–105.

Merton, R. C. (1976). Option pricing when underlying stock returns are discontinuous. *Journal of Financial Economics, 3*, 125–144.

Oh, D. H., & Patton, A. J. (2012). Modelling dependence in high dimensions with factor copulas. Manuscript, Duke University.

Sato, K. (1999). Lévy processes and infinitely divisible distributions. Cambridge studies in advanced mathematics: 68. Cambridge University Press.

Shevchenko, P. V. (2006). Implied correlation for pricing multi-FX options. *Derivatives Week* March 13 pp. 8–9, March 20 pp. 10–11.

Tankov, P. (2004). *Lévy process in finance: Inverse problems and dependence modelling, Ph.D. thesis*. Paris: Ecole Polytechnique.